

**The author(s) shown below used Federal funds provided by the U.S. Department of Justice and prepared the following final report:**

**Document Title:           Improvements in Laser Ablation-Inductively  
Coupled Plasma-Mass Spectrometry for  
Forensic Analysis**

**Author(s):                 Megan L. Mekoli, Jonna Berry, Stanley J. Bajic,  
R. S. Houk**

**Document No.:           242953**

**Date Received:          July 2013**

**Award Number:          2009-DN-R-112**

**This report has not been published by the U.S. Department of Justice. To provide better customer service, NCJRS has made this Federally-funded grant report available electronically.**

<p><b>Opinions or points of view expressed are those of the author(s) and do not necessarily reflect the official position or policies of the U.S. Department of Justice.</b></p>
---

## **PROJECT TITLE**

IMPROVEMENTS IN LASER ABLATION-  
INDUCTIVELY COUPLED PLASMA-MASS SPECTROMETRY  
FOR FORENSIC ANALYSIS

## **AWARD NUMBER**

2009-DN-R-112

## **AUTHORS**

Megan L. Mekoli, Jonna Berry, Stanley J. Bajic<sup>a</sup> and R. S. Houk<sup>b</sup>

a. Ames Laboratory, U. S. Dept. of Energy, Ames, IA 50011, (515)294-2086,  
[sjbajic@ameslab.gov](mailto:sjbajic@ameslab.gov)

b. Ames Laboratory USDOE, Dept. of Chemistry, Iowa State University, Ames IA  
50011

515-294-9462 [rshouk@iastate.edu](mailto:rshouk@iastate.edu)

## ABSTRACT

Laser ablation inductively coupled plasma – mass spectrometry (LA-ICP-MS) was evaluated for elemental analysis of tapes and copper wires for forensic comparison purposes. Both a conventional 10 ns laser and a short pulse (100 fs) laser were used. Principal components analysis (PCA) was used for data interpretation and for pairwise comparisons of samples based on elemental composition.

The main findings from this project are as follows.

1. Some elements were distributed heterogeneously in the copper wire samples, especially elements at low concentrations. The section analyzed must be large enough to minimize this problem, which limits the applicability of the technique for very small samples.
2. Many brands of tape samples could be discriminated readily.
3. PCA methods that employ biplots for determining which elemental signals contribute the most to the overall signal variance can be used to derive additional information from pairwise comparisons.
4. Large differences in performance between the ns and fs laser were not observed for the copper wire samples. The fs laser ablated through the tape samples very rapidly, which precluded separate analysis of the back and adhesive sides with this laser.
5. It was difficult to ablate only the adhesive side of tape because the laser removes some of the underlying substrate as well.

**TABLE OF CONTENTS**

ABSTRACT	2
EXECUTIVE SUMMARY	4
INTRODUCTION	5
PROGRESS PART I - TAPE ANALYSIS	8
Abstract	9
Introduction	10
Methods	13
Results & Discussion	18
Conclusion	39
PROGRESS PART II - COPPER WIRE ANALYSIS	
Abstract	41
Introduction	42
Methods	45
Results & Discussion	52
Conclusion	67
DISSEMINATION OF RESEARCH FINDINGS	69
REFERENCES	70

## EXECUTIVE SUMMARY

LA-ICP-MS is a minimally-destructive method for trace elemental analysis of solids. A solid sample is ablated with a laser, which produces particulates. The sample particulates are transported in a gas stream into an argon inductively coupled plasma (ICP, temperature  $\sim 7000$  K), where the particulates are heated and converted into atomic ions. The ions are then extracted into a mass spectrometer (MS), which separates ion based on their mass-to-charge ratio ( $m/z$ ). Since the ions are almost completely atomic, the  $m/z$  values where peaks appear identify the elements based on their known isotope abundances. The peak heights are proportional to the element concentrations. ICP-MS is a rapid and highly sensitive technique, which can detect sub- ppb levels of many elements.

The general goal of this project was to improve the performance of LA-ICP-MS to identify and quantify elements for forensic analysis of important sample types not readily amenable to existing methods. These samples were of two major types: a ) electrical and duct tapes, and b) copper strands in multi-stranded wires, both of which are commonly used in crimes, e.g., for binding victims or as components of bombs. These “soft” samples are prone to heating and melting by conventional laser pulses, which leads to fractionation effects that reduce analytical accuracy. Ultraviolet (wavelength 266 nm) lasers with two different pulse lengths were used: a conventional 10 nanosecond (ns) laser and a new 100 femtosecond (fs) laser. Unfortunately, the fs laser burned through the tape samples too fast to allow separate analysis of the back and adhesive sides. For the copper wire samples, large differences in sensitivity or in the relative abundances of different elements were not observed using the two lasers.

The elemental data obtained were compared rigorously by principal components analysis (PCA). The PCA process yields  $Q$  residual values, which are

systematic measures of the distance between separate groups of data points. A novel way to extract comparison information during PCA comparisons by use of biplots was investigated. Basically, biplots allow identification of which elements contribute most extensively to observed differences in elemental composition of two similar samples. In some cases, these distinctive elements can be correlated with important characteristics of the samples, e.g., with details of the manufacturing process.

The main finding from the copper wire analysis was that the trace elements were not distributed uniformly with respect to spatial position. Initial measurements of only small sections of individual strands indicated they had different composition and thus could be distinguished. However, repeating the measurements while ablating longer sections of various strands led to larger uncertainties and fewer distinctions between strands. The same effect was seen a) when sections of the strands were dissolved, and b) when either the fs or ns laser were used, so this is not a problem with laser ablation per se. Thus, ablating enough material to generate a representative sample is an important requirement. This spatial heterogeneity of trace elements is likely to be a more common problem when a) the samples are highly pure materials (like the copper wires), b) when elements at lower concentrations are measured, and/or c) the amount of sample material is small, as was the case for these thin copper wires.

## INTRODUCTION

### Statement of Problem & Research Hypothesis

Various tapes and strands of copper wire were selected for elemental analysis. These items are commonly used in crimes; matching or distinguishing them based on their elemental composition could be useful for forensic purposes. Preliminary data gathered for the original proposal indicated that different wires and tapes had distinguishable elemental compositions. The basic hypothesis was that the origins of various brands of these materials could be deduced from trace element analysis by LA-ICP-MS. A more thorough assessment of this hypothesis was conducted.

### Literature

Conventional ICP-MS requires the sample to be in solution. Although such dissolution procedures are desirable in many scientific applications, they destroy the original solid sample, which is undesirable in forensics. LA-ICP-MS has these desirable features: the solid sample is analyzed intact, and lateral spatial resolution is also possible. This technique has been used for attribution purposes in forensic situations, with good performance.<sup>1,2</sup> Compared to other methods for nondestructive elemental analysis, primarily X-ray fluorescence, LA-ICP-MS has much better detection limits. Low abundance elements can be seen with ICP-MS, which improves the specificity and distinction ability for attribution. ICP-MS can also measure isotope abundances, which provides additional information, especially for elements like Li, Pb and U, whose isotope ratios vary substantially.

However, a large body of work has shown that the ~10 ns pulsed UV lasers commonly used in LA-ICP-MS have an important weakness. Briefly, they melt part of the sample, rather than cleanly ablating it into the gas phase. The gas phase

atoms condense quickly into particulates that are then carried into the ICP. This melting can result in problems like a) differences in the elemental composition of the resulting particulates from that of the original sample, and b) changes in composition of the ablated particulates with time during ablation, even when the sample is spatially homogeneous.<sup>3</sup> Russo et al. demonstrated substantial improvements using a much shorter (~ 100 fs) laser pulse.<sup>4,5</sup> Other groups have corroborated and extended Russo's observations,<sup>6,7,8</sup> including our own fast photographic studies of particle clouds in the ICP.<sup>9,10</sup> The improvements are particularly notable for metals,<sup>4,5,11</sup> whose high thermal conductivity makes them prone to heating and melting effects.

## **Research Rationale**

The results are discussed below separately for each sample type, as the preparation and data analysis methods differed somewhat.

**Progress Part I**

**Iterative Subtraction and Principal Component Analysis of the Trace  
Elemental Composition of Duct and Electrical Tapes**

## ABSTRACT

Tape can be used to commit a crime, e.g., to bind or gag a victim, and is often collected as crime scene evidence. The elemental composition of tape is thus of forensic interest. Elemental measurements of duct and electrical tapes were taken by nanosecond laser ablation-inductively coupled plasma-mass spectrometry. Principal component analysis (PCA) is a multivariate data reduction technique used to simplify and visualize large sets of data. The data collected were analyzed using PCA. An iterative subtraction technique is used to determine which elements contribute the most variance between differing brands of each type of tape; it is likely that some of these elements originate from bulk additives during the manufacturing process of these tapes. The adhesive and backing sides from four different brands of duct and electrical tape are analyzed using PCA and the iterative subtraction technique described. Head-to-head comparisons of these tapes are performed using Q-residual analysis. All brands of the backing and adhesive sides of duct tape were found to be distinguishable from one another to 95% confidence. Similarly, the backing side of all brands of electrical tape analyzed were distinguishable from one another to 95% confidence. The adhesive side of Plymouth brand electrical tape could not be distinguished from those of UL and Super 33 brands.

## INTRODUCTION

Duct and electrical tapes are often collected from crime scenes as evidence. These tapes can be used to commit a crime and may be found in bombs or from binding a victim. The composition of such a tape sample could be of forensic interest as new methods for pairwise comparisons become available.

Searchable databases of common forms of evidence are desirable to law enforcement officials. Databases could include the trace composition of objects commonly used to commit a crime. However, the creation and management of such a database is an exhaustive task that requires extensive time and funds. Trace analysis of tape and other materials of forensic interest (paints, glass, metals, fibers, etc.) may be accomplished by elemental analysis without quantification using statistics. Qualitative pairwise comparison is direct matching of evidence collected at a crime scene to a small set of candidate samples collected from a suspect. To prove a match using this type of analysis, forensic analysts must show that the evidence is distinctive. Statistical analysis of trace components in evidence can be used to determine the level of confidence a forensic scientist has in attributing the evidence from the crime scene to a similar candidate sample.

Characterization and attribution of tapes as forensic evidence has been done by end matching<sup>12</sup> and microscopic evaluation methods.<sup>13, 14, 15</sup> Recently, trace metals and organic components in electrical tape have been measured using attenuated total reflectance-fourier transform infrared spectroscopy (ATR-FTIR), X-ray fluorescence (XRF), and middle infrared spectroscopy (MIR-IR).<sup>15, 16, 17, 18,</sup> Goodpaster<sup>17, 18</sup> published a comprehensive study of electrical tapes using scanning electron microscopy with energy dispersive spectroscopy (SEM-EDS) and X-ray powder diffraction (XRPD) instrumental techniques. Goodpaster also only measured the signals from 10 elements that could readily be seen using SEM-EDS.

SEM-EDS has a detection limit of approximately 10 ppm, which is not sensitive enough for the detection of ultratrace elements. There has not been elemental analysis of duct tape in the literature to date.

Compared to most samples analyzed by LA-ICP-MS, tape is thin and prone to melting, stretching and weathering, which makes it a difficult medium to analyze. Non-destructive techniques such as SEM-EDS and XRF contain desirable attributes for analysis, however these methods lack the sensitivity to measure ultratrace components in tape at concentrations of 10 ppb or lower. High sensitivity and the ability to rapidly analyze the trace element composition of tape sets laser ablation inductively coupled plasma-mass spectrometry (LA-ICP-MS) apart from methods used in the literature.

### ***Laser Ablation ICP-MS***

Dissolution of a tape sample for analysis of trace components via ICP-MS accomplishes the sensitivity needed for ultra-trace forensic analysis, but completely destroys precious evidence. Laser ablation (LA) is a sampling technique that uses a laser (usually in the ultraviolet) to ablate a small amount of material from the sample surface for analysis by the ICP-MS device. LA-ICP-MS is a rapid and sensitive technique, which causes only minor sample destruction, requires no sample preparation, and is capable of measuring analytes in concentrations of 10 ppb or lower. Gray<sup>19</sup> was the first to combine the high sensitivity and multielement measurement capabilities of the ICP-MS with a laser, for direct sampling of solid materials. Watling became the first to use LA-ICP-MS for forensic purposes by analyzing trace elements in gold.<sup>1</sup> Other forensic uses of LA-ICP-MS are to match fragments of glass,<sup>20, 21, 22</sup> fingerprint sapphires,<sup>23</sup> and compare brick stones<sup>24</sup> among many other areas of trace forensic science.

### *Principal Components Analysis*

Multivariate statistical techniques are valuable to manage the analysis of the large sets of information produced by ICP-MS. Principal components analysis (PCA) is a statistical data reduction technique which examines variance in complex multidimensional datasets and allows for graphical visualization of groupings and trends.<sup>20, 25</sup> To visualize these groupings and trends, multiple data collections from each sample are required to gain a clear understanding of the content for each sample. Different analyses of the same sample should have similar characteristics as each other, whereas analyses of different samples may have widely varying characteristics from one sample to another.

PCA was previously used to analyze data collected from laser ablation ICP-MS measurements of glass fragments and metals.<sup>21, 26</sup> Goodpaster et al. have also published statistical analyses of electrical tape using PCA<sup>17, 18</sup> and found it was a very useful tool for analyzing multi-element data using SEM-EDS. However, Goodpaster et al. measured signals from only 10 elements. Using PCA, Goodpaster et al. were able to distinguish 36 different classes (i.e. brands and dates of manufacture) of electrical tapes from one another.

Thus far, the analytes measured for head-to-head comparison of tapes in the literature have only been ones that are relatively abundant. Because the techniques mentioned in the literature are not sensitive enough to measure ultratrace elements, only 10 elements that are expected to be present in all tapes have been examined. Goodpaster reported that lead content was one important distinguishing characteristic between different electrical tapes. In 2002, lead was discontinued as a component in the production of these tapes. Therefore, tapes manufactured prior to 2002 should contain more lead. However, if the sample set is composed only of

tapes manufactured prior to 2002 or after 2002, the tapes are not so easily distinguished from each other. While Goodpaster et al. were able to distinguish 36 classes of the analyzed electrical tapes from one another, perhaps more detailed information for pairwise comparison could be gained by measurement of more elements using ICP-MS. Duct tape has not been previously examined in this way.

Ultratrace elemental analysis could help distinguish two otherwise indistinguishable samples of tape. The work described here provides a method by which elemental trace analysis may be conducted to determine which elements in tapes provide the most variability on an individual case-by-case basis.

## **METHODS**

### *Samples*

Duct tape is manufactured by combining a scrim (or cloth) to a polyethylene back using a poured, hot rubber adhesive. Electrical tape is manufactured by spraying hot adhesive onto a polyvinyl backing.<sup>27, 28</sup>

Table 1 is a list of samples that were used in this study. Exact dates of manufacture were unknown. Two separate rolls of 3M Super 33 electrical tape were analyzed. One was a newer roll that had been manufactured in the early 2000s and the other roll was approximately 20 years older. Both Super 33 rolls were included in the study to determine whether tapes manufactured several years apart by the same company could be distinguished.

**Table 1** List of pressure sensitive tapes analyzed

Tape	Identifier	Manufacturer
Duct		
	Duck	ShurTech Brands, LLC
	3M	3M Company
	Nashua	Tyco Adhesives
	Staples	Staples, Inc.
Electrical		
	Super 33	3M Company
	Old Super 33	3M Company (manufactured before 2000)
	Plymouth	Plymouth Rubber Co. Ningbo Universal Tools Co, LTD
	UL	

***Laser Ablation and ICP-MS***

The outer layer of tape still on the roll is likely contaminated, so several layers were unrolled and discarded to expose fresh tape underneath. A fresh tape sample approximately 7 cm long was cut, stretched across a large metal washer (4.4 cm outer diameter) to support the tape in the LA cell, and the excess tape was trimmed off. The backing and adhesive sides were ablated in a square raster pattern through the hole in the washer; the underlying washer was not ablated. A medium

resolution ( $m/\Delta m = 4000$ ) full mass spectrum ( $m/z = 7$  to 238 except for  $m/z$  10 to 23, 32 to 45, 54, 79 to 82, 127, 129, 151, and 210 to 231) was acquired by a magnetic sector ICP-MS device (ELEMENT 1, Thermo Fisher Scientific Inc., Bremen Germany), which has been described elsewhere.<sup>29</sup> Mass spectra were collected from seven different spots on each side of a tape sample while ablating a square raster pattern on the surface of the sample. The interior of the ablation cell was wiped with a clean, dry kim wipe whenever the cell was opened to flip the washer or to change samples. Background signals were collected with argon flowing through the ablation cell while the laser was off.

Samples were ablated using a commercial Q-switched Nd:YAG laser (266 nm, frequency quadrupled from 1064 nm, pulse length 10 ns, pulse energy 9 mJ, CETAC LSX 500, CETAC Technologies, Omaha, NE). Laser and ICP-MS parameters may be found in Table 2. The signals at each  $m/z$  value were peak-area integrated and background subtracted. In general, signal ratios corresponded to accepted isotope ratios.

We attempted to select laser parameters to remove only one side of the samples. Visual inspection after ablation indicated that the laser did not dig completely through the sample. When the backing side was ablated, little or none of the underlying adhesive was removed. The tape samples were also ablated with the adhesive side exposed to the laser. In this case it was difficult to remove only the adhesive without some of the backing as well.

### *Data Analysis*

PCA was performed using the peak integrated and background subtracted signals at various  $m/z$  values with commercial software (Solo Eigenvector versions 4.0 and 6.3). To avoid biasing the data, other preprocessing procedures such as normalizing, mean centering, or autoscaling were not done before PCA.

**Table 2** Instrument and laser parameters for the analysis of duct and electrical tapes

ICP-MS Instrument	ELEMENT 1 (Thermo Scientific, Inc.)
10 ns Laser	CETAC LSX 500 Nd:YAG
Operational wavelength	266 nm
Laser energy	9.1 mJ pulse <sup>-1</sup>
Frequency	20 Hz
Spot size	100 μm
Raster speed	350 μm sec <sup>-1</sup>
Sampler and skimmer cones	Ni, H configuration (Thermo Scientific, Inc.)
Sample gas	1.06 L Ar min <sup>-1</sup>
RF Power	1150 W
Outer/auxiliary gas stream	16.00/1.16 L Ar min <sup>-1</sup>
Torch position, ion optics	Optimized for maximum sensitivity and stability
Scan mode dwell/settling time	Peak jump, 10 points per mass, 10 ms dwell time, 2.1 ms settling time
Acquisition Runs/passes	3 runs/1 pass
Elements measured (medium resolution)	Li, Mg, Al, P, Sc, Ti, V, Cr, Mn, Fe, Co, Ni, Cu, Zn, Ga, Ge, As, Se, Rb, Sr, Y, Zr, Nb, Mo, Ru, Rh, Pd, Ag, Cd, In, Sn, Sb, Te, Cs, Ba, La, Ce, Pr, Nd, Gd, Ho, Hf, Ta, W, Re, Os, Ir, Pt, Au, Hg, Tl, Pb, Bi, Th, U

## RESULTS AND DISCUSSION

Figure 1 compares peak integrated background subtracted mass spectra from two measurements of the adhesive sides of two different duct tape samples. In this case the spectra are different enough to be distinguished visually, but this is often not so

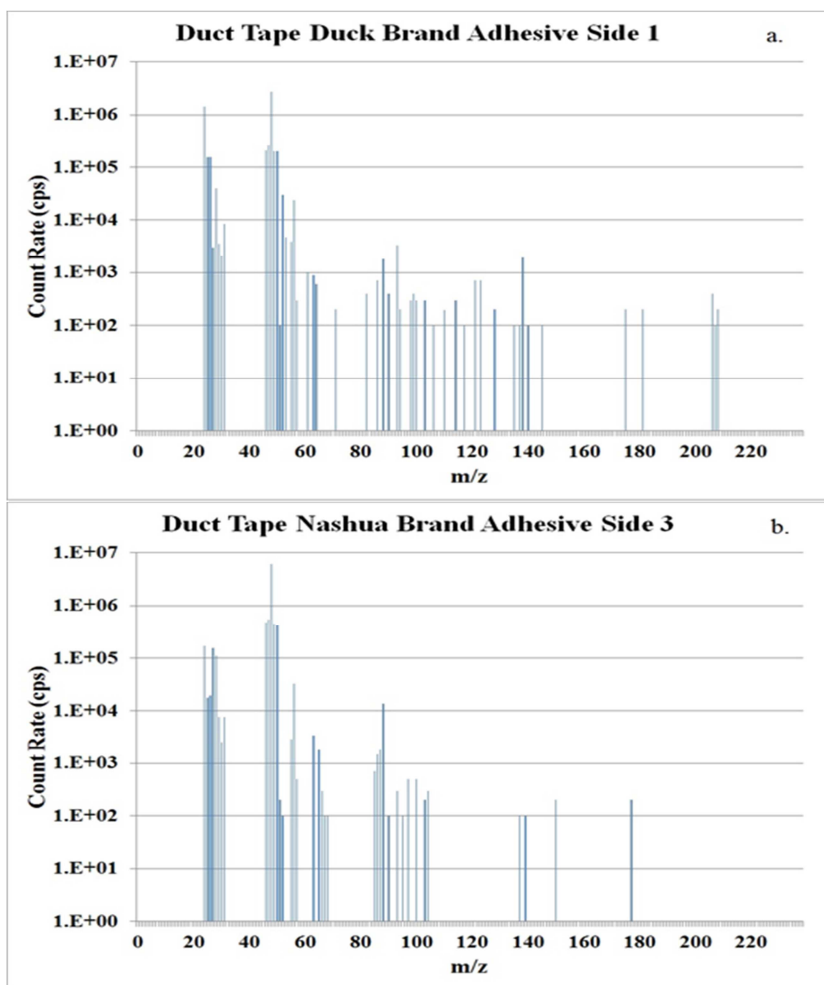


Figure 1 Mass spectra for adhesive side sampling for two brands of duct tape. a. first sampling of Duck brand duct tape and b. third sampling of Nashua brand duct tape.

PCA is a multi-dimensional data reduction technique using matrix mathematics to optimize variance patterns within a large dataset.<sup>30,31</sup> PCA reduces the dataset into fewer dimensions, which can be easily plotted and highlights the differences and similarities between samples. All the original information is retained; it is simplified, and different data sets can be compared more easily.

A model is a specific set of mathematical equations that describe the reduction of one particular dataset. Different models (equations) describe different sets of data. Each equation is called a principal component. There can be multiple principal components which best describe a particular dataset. These principal components are ranked by how they best describe the differences between the samples (PC1, PC2, PC3, etc.). A score is one solution to a principal component. Each sample will have one score for each principal component. If two samples are different, they will have two different scores for at least one principal component. Typically, one entire dataset will be reduced to two principal components that highlight the largest differences between the samples. The scores may be plotted in a coordinate plane called a scores plot to visualize how the different samples relate to one another.

A Q-residuals plot can also be used to compare how the variables (in this case, mass spectra) of each of the different brands relate to one another. A model can be created for the values of one particular subset of data (such as the mass spectra taken of different ablated spots for one particular brand of tape) within the whole dataset. The brand used as the model may be compared to all other brands. A plot of the average Q-residuals between the sample and model data represents a comparison of the averaged mass spectrum of the sample to that of the model. A large numerical Q value indicates the samples differ extensively. A 95% confidence interval may be generated from basic Gaussian statistics using the

analyzed data for each separate model. The 95% confidence interval Q-value may then be plotted onto the average Q-residuals plot. Samples lying above the 95% confidence interval line are called “distinguishable from the model (to 95% confidence)” and samples lying below the 95% confidence interval are said to be indistinguishable from the model (to 95% confidence).

### ***Variance, Biplots, and Iterative Subtraction Process***

Variance is described here as the difference between groups of sample scores compared to the span of one single group of scores. Particular variables (in this case, isotope m/z values) that contribute the most to the overall variance between samples may be identified using a biplot and a process called iterative subtraction.

Iterative subtraction is a process of repeatedly identifying and removing the variables and their data which contribute the most variance to the model sample scores. This process is illustrated below for a dataset pertaining to the analysis of the backing side of duct tape (Figure 2). PCA makes a model ( $T_0$ ) for that dataset ( $[d_0]$ ) that creates the largest variance between groups of samples. In the simplest of forms, PCA can be represented by the following:

$$T_0[d_0] \quad [1]$$

A scores plot (Figure 2) is the visual result of the model applied to that dataset. In Figure 2, the majority of the variance (99.93%) in the sample scores is captured by principal component 1 (PC 1) leaving only 0.07% of the total variance remaining. PC 2 captures the majority of the remaining variance (0.06 %). In this particular scores plot, there are distinct groups which correspond to the different brands of duct tape analyzed.

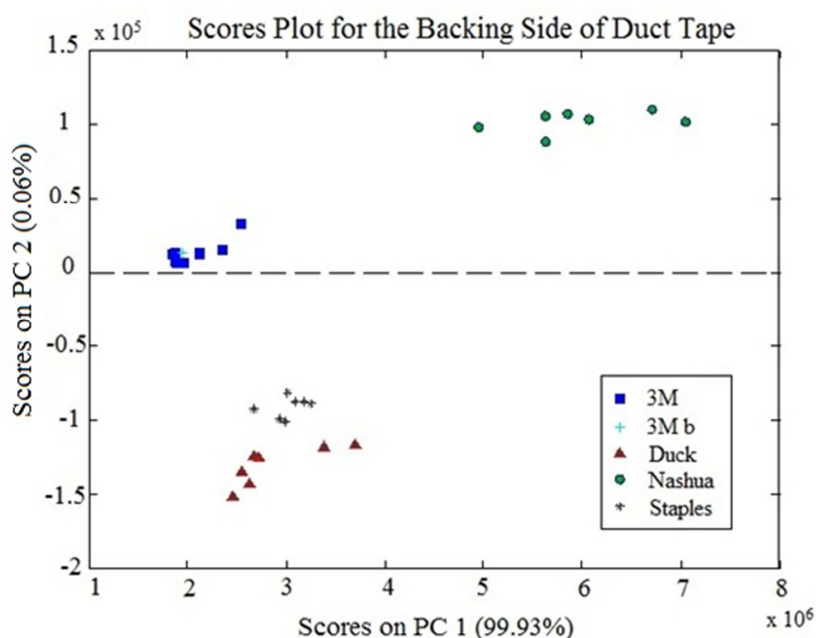


**Figure 2** Scores plot for the backing side of duct tape. All data collected corresponding to all elements measured was used to create the scores plot shown above. The numbers in the parentheses indicate the amount of variance captured in the principal component. The model was based on all data collected for all elements measured. The point labeled “3M b” was an extra point analyzed at the end of the experiment to monitor instrumental drift.

A biplot can be used to identify those variables ( $m/z$  values) that contribute the most variance to the observed separation of sample groupings.<sup>32</sup> To create a biplot, the same model used to make the scores plot ( $T_0$ ) is applied to the set of isotopic  $m/z$  variables themselves ( $[M_0]$ ). These variables will have their own scores for each principal component, which in turn may be plotted.

$$T_0[M_0] \quad [2]$$

The plot of  $T_0[M_0]$  is overlaid onto the scores plot to form a biplot. A biplot is a visual representation showing which isotopes have the largest contribution to the variance between samples. Isotopes which lie furthest from the origin of the biplot were most influenced by the model and therefore contribute the most to the variance between the samples in the dataset.

Figure 3 is the biplot determined from the data used in the scores plot (Figure 2) for the backing side of duct tape. The point furthest from the origin corresponds to the mass spectral peak at  $m/z$  27 or  $^{27}\text{Al}$ . In this example,  $^{27}\text{Al}$  is the only discernible isotope that is separated from the origin. The signal for  $^{27}\text{Al}$  contributes the most to the observed differences between the samples (Figure 2). Other elements could also be important, but the scale is such that only  $^{27}\text{Al}$  stands apart.

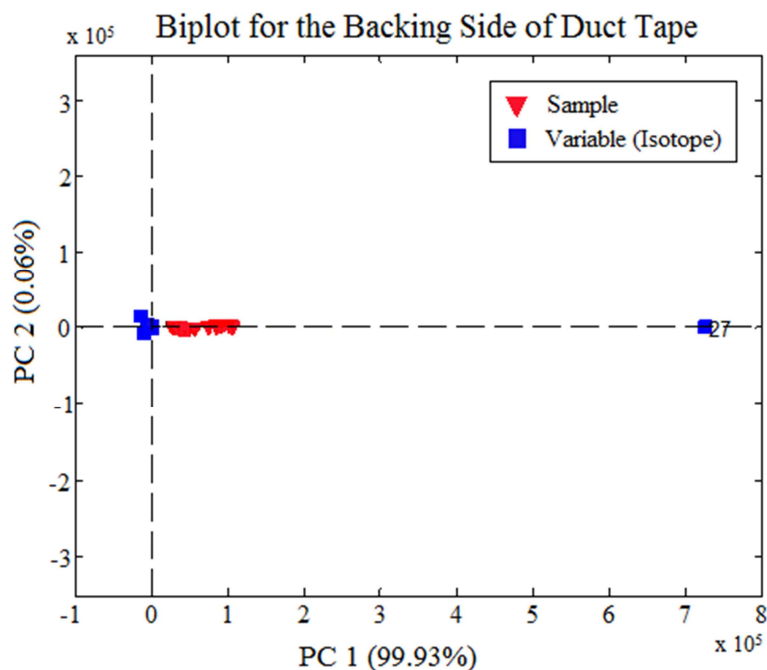


**Figure 3** Biplot for the backing side of duct tape showing the 1st order of variance. This plot was achieved by overlaying the variable axes onto the scores plot found in Figure 2. Variables (in this case isotope masses, blue squares) which contribute the most variance to the separation of the samples (red triangles) lie farther away from the origin. Isotope mass 27, corresponding to Al, contributes the most variance to the sample scores.

In order to determine which other elements contribute significant variance, the data corresponding to Al and the Al variable itself were removed from both the

dataset and the  $m/z$  variables. Data for all isotopes of each element that contributed significant variance were eliminated to avoid confusion between minor isotopes of larger variance contribution and major isotopes of lower variance contribution. The first discernible element(s) removed are considered to be the first order variance; in this case, Al is the only element removed as the first order variance.

In Figure 3, the points for the isotopes other than  $^{27}\text{Al}$  cluster around the origin of the biplot. In the next step, a new model ( $T_1$ ) was applied to the new dataset ( $d_1$ ) to maximize the variance between the samples. A new biplot from the remaining isotope  $m/z$  variables results with the 1<sup>st</sup> order data and variables removed.

$T_1[d_1]$  scores plot (Figure 4) [3]

$T_1[M_1]$  biplot (Figure 5) [4]

A second model ( $T_1$ ) may be applied to the new dataset for these remaining elements ( $[d_1]$ ) and a second scores plot (Figure 4) was plotted. In Figure 4, various tape samples are still separated, even though the data for the most distinctive element ( $^{27}\text{Al}$ ) have been removed.

A second biplot (Figure 5) may be constructed by overlaying axes of the remaining isotopes onto the scores plot. The points in Figure 5 corresponding to isotopes  $^{24}\text{Mg}$ ,  $^{115}\text{In}$ ,  $^{56}\text{Fe}$  and  $^{76}\text{Se}$  may be discerned from the large group of points and elements. These four elements make up the second order of variance. Their signals account for most of the remaining variance. Thus, the use of biplots identifies the elements most responsible for the observed differences between samples. This information is not normally present in either scores plots (e.g., Figs. 2 and 4) or Q-residual plots.

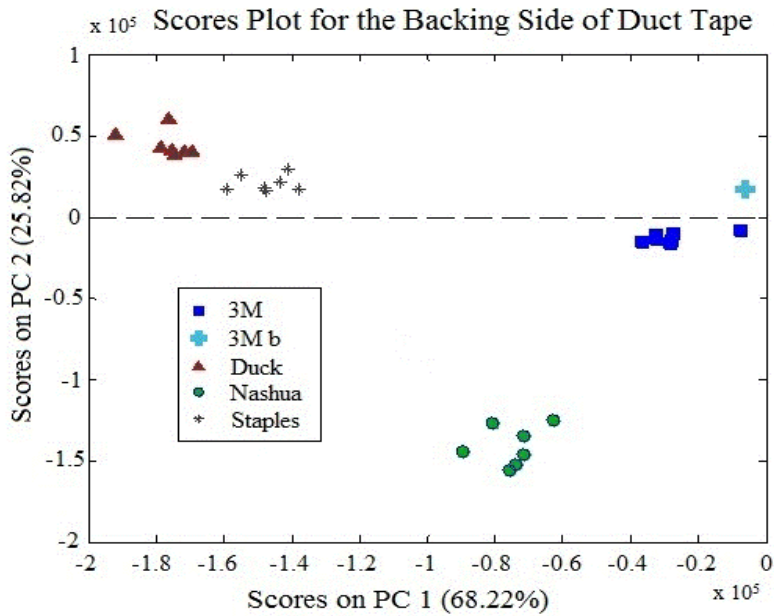


**Figure 4** Scores plot for the backing side of duct tape after the element(s) corresponding to first order variance has been removed.

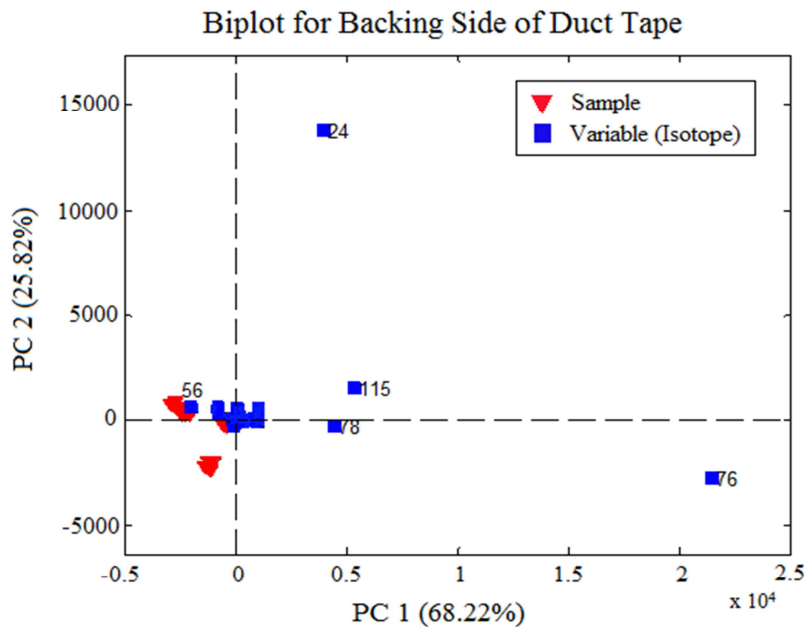


**Figure 5** Biplot showing the 2nd order variance for the backing side of duct tape. Variables (isotope masses, blue squares) contributing the most variance to the sample scores (red triangles) are labeled above. Isotope mass 24 corresponds to Mg, 115 corresponds to In, 76 and 78 correspond to Se, and 56 corresponds to Fe.

Next, the data for these 2<sup>nd</sup> order elements were removed.

$T_2[d_2]$  scores plot (Figure 6) [5]

$T_2[M_2]$  biplot (Figure 7) [6]

A third scores plot (Figure 6) was created using the edited model ( $T_2$ ) and dataset ( $[d_2]$ ). The third scores plot in Figure 6 indicates that there is much less variance between samples as there are fewer distinct groups of separate samples. The third biplot (Figure 7) that was constructed shows which elements make up most of the remaining variance;  $^{52}\text{Cr}$ ,  $^{48}\text{Ti}$ ,  $^{49}\text{Ti}$ ,  $^{63}\text{Cu}$ , and  $^{65}\text{Cu}$ .

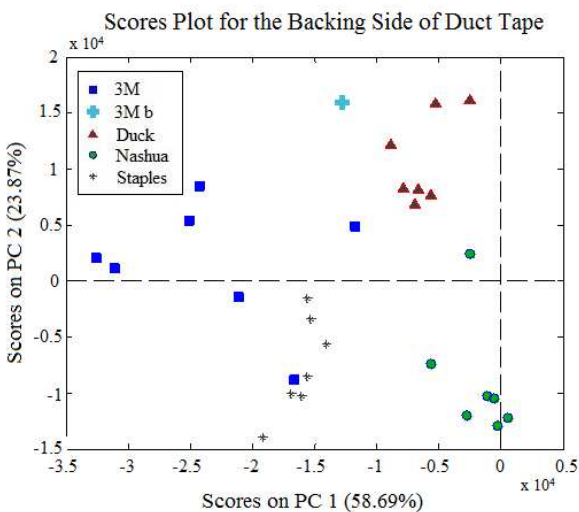


Fig. 6

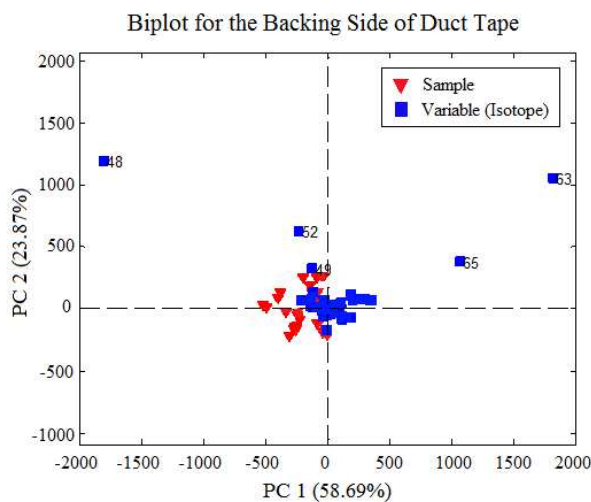
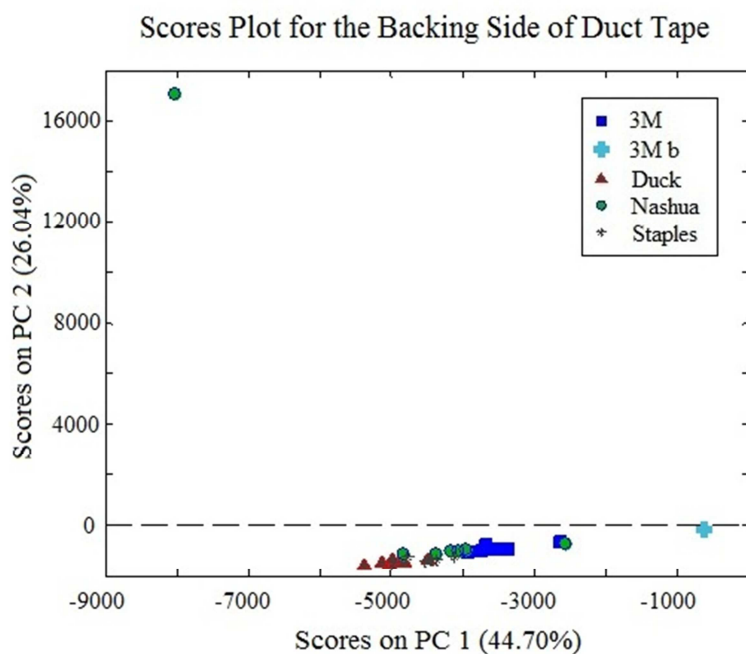


Fig. 7

**Figure 6** Scores plot with data corresponding to the 1st and 2nd orders of variance removed for the backing side of duct tape.

**Figure 7** Biplot showing the 3rd order variance for the backing side of duct tape. Variables (isotope masses, blue squares) contributing the most variance to the sample scores (red triangles) are labeled above. Isotope mass 48 corresponds to Ti, 52 corresponds to Cr, and both 63 and 65 correspond to Cu.

This process of iteratively subtracting the data and elements which contribute the most amount of variance is repeated until the new model no longer distinguishes between the different samples. Figure 8 is a scores plot after data corresponding to elements in the first three orders of variance (Al 1<sup>st</sup> order; Mg, Fe, Se and In 2<sup>nd</sup> order; and Ti, Cr and Cu 3<sup>rd</sup> order) have been removed. Distinct groupings of the samples cannot be visualized in Figure 8, indicating there is little variance left between the samples. In this example, isotopic signal data for the remaining 47 elements either does not vary from sample to sample, or corresponds to low-level noise fluctuations from the instrument.



**Figure 8** Scores plot for the backing side of duct tape after data for elements corresponding to the first three orders of variance have been removed.

At this point, the removed data were combined into a final dataset  $[d_f]$  upon which a final model ( $T_f$ ) was applied. Data for the  $m/z$  values other than these identified in the 1<sup>st</sup> – 3<sup>rd</sup> orders were not present in  $[d_f]$ .

$T_f[d_f]$  final scores plot (Figure 9)

[7]

The final scores plot in Figure 9 is very similar to the initial scores plot (Figure 2), indicating that only the data from elements contained in the first three orders of variance were necessary to accurately compare this set of samples.

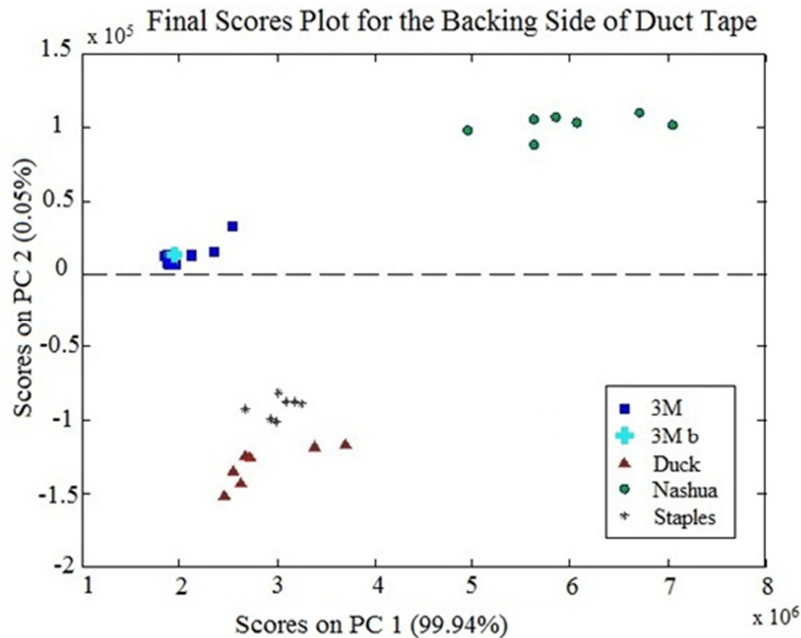


**Figure 9** Final scores plot for the backing side of duct tape using data only from elements in the 1st, 2nd and 3rd orders of variance.

This iterative subtraction technique was used to determine which elements contribute most to the observed variance between samples of two kinds of the tape (duct and electrical), both adhesive and backing sides. Elements were removed and grouped in order of decreasing contribution to the variance between the brands until the various samples could no longer be distinguished. In the case of all tapes analyzed, only three consecutive orders of element classification using scores plots and biplots were necessary.

### ***Duct Tape, Backing Side***

Figure 9 is the final scores plot ( $T_f[d_f]$ ) for measurements taken from the backing side of four separate brands of duct tape after elements in the 1<sup>st</sup>, 2<sup>nd</sup>, and 3<sup>rd</sup> orders of variance were identified from the biplot process. The separations in scores of one group from those of members of a different group indicate that the samples within the first group can be distinguished from the second group based on the acquired mass spectra. Points on the scores plot which appear to overlap indicate the samples are not distinguishable from one another based upon the acquired mass spectra.

Biplots were constructed from the scores data and the iterative subtraction technique was applied. The elements found in the orders of variance table (Table 3) correspond to the elements which contribute the most variance between the different brands. Aluminum is a bulk additive in duct tape to achieve the silver hue of the backing.<sup>27</sup> If Al is present in all duct tapes, it is not expected to be distinctive. However, the high variance in Al abundance between different duct tape brands indicates that different manufacturers add Al in widely varying amounts to give the tape silver hues that are distinct from other manufacturers' products. Al is also typically added to the adhesive side of duct tapes as kaolinite ( $Al_2Si_2O_5(OH)_4$ ) during the manufacturing process to add volume, reinforce the rubber adhesive or add color.<sup>27</sup> Magnesium likely comes from talc ( $Mg_3Si_4O_{10}(OH)_2$ ), which is added to duct tapes for strength and to make them water repellent. Titanium likely originates from  $TiO_2$ , which may leak into the backing side from the adhesive side, as it is a common component in duct tape adhesives.<sup>27</sup> Iron could be present from tape contact with metal parts during the manufacturing and packaging process or may have been an inorganic additive by the manufacturers. The origins of In and Se are unclear.

Figure 10 is the average Q-residuals plot derived from the scores after the three orders of variance (Table 3) were combined. The separation in the variables is almost identical to those of the scores plot constructed prior to the iterative subtraction technique (data not shown). Scores for the subtracted elements of all brands were compared to those of the model brand. All average

**Table 3** Variance contribution of isotopes to the model for the backing side of duct tape. Signals for these isotopes were used to create the scores plot in Figure 9.

Order of Variance	Isotopes
1 <sup>st</sup>	$^{27}\text{Al}$
2 <sup>nd</sup>	$^{24}\text{Mg}$ , $^{56}\text{Fe}$ , $^{78}\text{Se}$ , $^{80}\text{Se}$ , $^{113}\text{In}$ , $^{115}\text{In}$
3 <sup>rd</sup>	$^{46}\text{Ti}$ , $^{47}\text{Ti}$ , $^{48}\text{Ti}$ , $^{49}\text{Ti}$ , $^{52}\text{Cr}$ , $^{53}\text{Cr}$ , $^{63}\text{Cu}$ , $^{65}\text{Cu}$

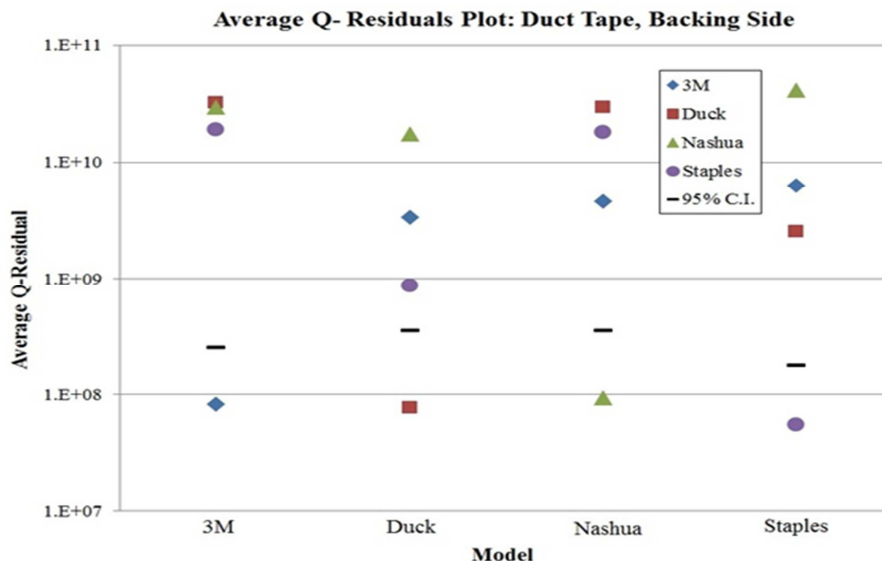


**Figure 10** Average Q-residuals plot for the backing side of duct tape. The black line denotes the 95% confidence interval for each model.

Q-values for each sample compared to each model are above the 95% confidence interval. The average Q-residuals plot in Figure 10 indicates that the backing sides of all brands of duct tape are distinguishable from one another to 95% confidence.

### ***Duct Tape, Adhesive Side***

Figure 11 is the scores plot for the adhesive side of duct tape using data only for elements from the first three orders of variance. This plot is similar to the original scores plot (not shown) that includes all data taken for all variables. Table 4 lists the orders for the elements; Al, Fe, Cu, Se, and In contribute the most variance between the brands on the adhesive side of duct tape. Again, Al is included as an element which contributes much variance in the first order. Large amounts of Al on the adhesive could be contamination from contact with the backing side while the tape was rolled up, or from unintentional sampling of the backing side while ablating the adhesive side. Due to the thinness of the adhesive layer, unintentional sampling of the backing side while ablating the adhesive side or vice versa could have been possible even though it was not specifically observed.

There are distinct groupings of ablated spots associated with each of the four brands in the scores plot in Figure 11. These scores were compared to one another using an average Q-residuals plot (Figure 12). In the Q-residuals plot (Figure 12), all points lie above the 95% confidence interval indicating all brands are distinguishable from one another to 95% confidence.

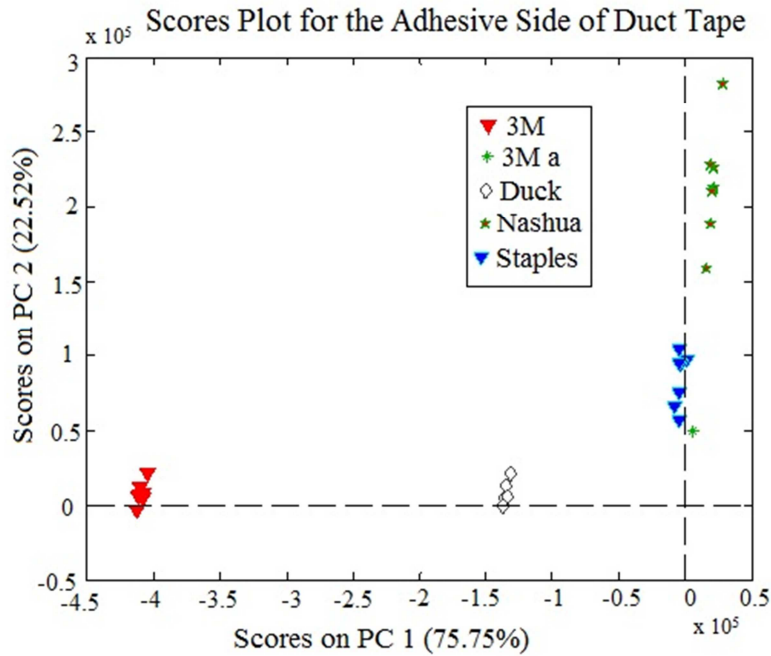


**Figure 11** Scores plot for the adhesive side of duct tape. The numbers in the parentheses indicate the amount of variance captured by each principal component. The model was based on elements contained in the first three orders of variance. The point labeled “3M a” was an extra point analyzed at the end of the experiment to monitor instrumental drift.

**Table 4** Variance contribution of elements to the model for the adhesive side of duct tape. Signals for these isotopes were used to create the scores plot in Figure 11.

Order of Variance	Isotopes
1 <sup>st</sup>	$^{27}\text{Al}$ , $^{56}\text{Fe}$ , $^{63}\text{Cu}$ , $^{65}\text{Cu}$ , $^{78}\text{Se}$ , $^{80}\text{Se}$ , $^{113}\text{In}$ , $^{115}\text{In}$
2 <sup>nd</sup>	$^{24}\text{Mg}$ , $^{46}\text{Ti}$ , $^{47}\text{Ti}$ , $^{48}\text{Ti}$ , $^{49}\text{Ti}$
3 <sup>rd</sup>	$^{31}\text{P}$ , $^{55}\text{Mn}$ , $^{52}\text{Cr}$ , $^{53}\text{Cr}$ , $^{78}\text{Sr}$ , $^{80}\text{Sr}$

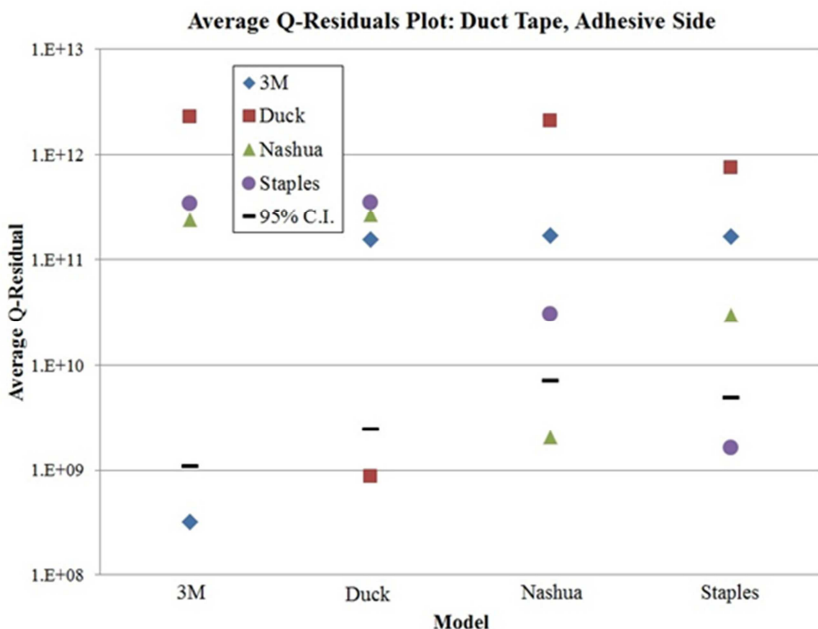


**Figure 12** Average Q-residuals plot for the adhesive side of duct tape. The black line denotes the 95% confidence interval for each model.

### *Electrical Tape, Backing Side*

Figure 13 is the scores plot for the backing sides of electrical tape using only those elements identified by the iterative subtraction technique. Table 5 lists elements contained in the first three orders of variance for the backing side of electrical tape. From Table 5, Pb and Sb contribute the most variance between the brands. Pb was once used in electrical tape as plasticizer.<sup>27</sup>

The amount of Sb detected could be from antimony oxide ( $\text{Sb}_2\text{O}_3$ ), which is a common inorganic additive to electrical tape backing.<sup>27</sup> Titanium is another common inorganic additive to electrical tapes, which can be incorporated as titanium oxide ( $\text{TiO}_2$ );<sup>27</sup> however, its abundance was found to vary less than that of Sb and Pb between the brands analyzed.

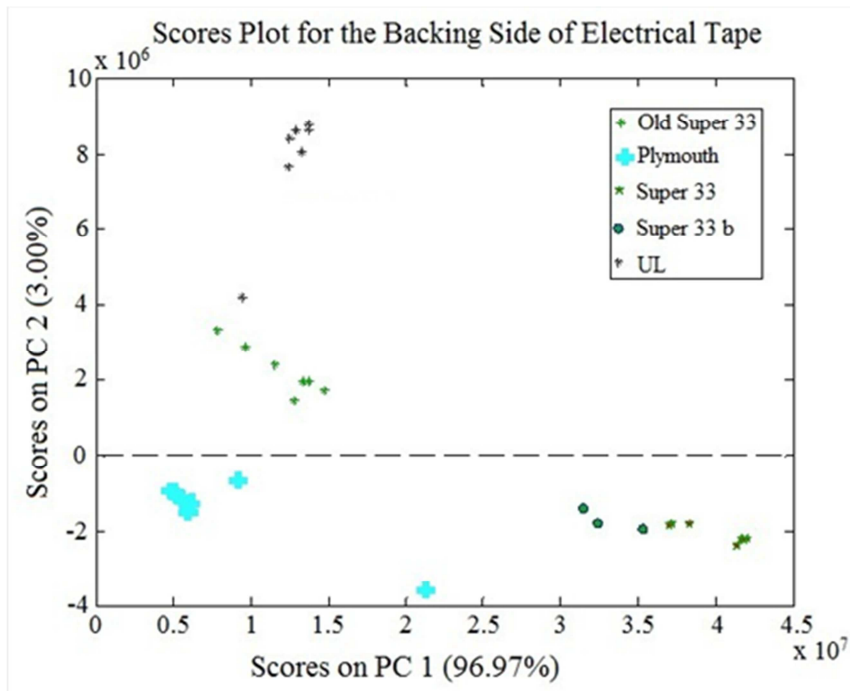


**Figure 13** Scores plot for the backing side of electrical tape. The numbers in the parentheses indicate the amount of variance captured in the principal component. The model was based on elements contained in the first three orders of variance (Table 5).

**Table 5** Variance contribution of elements to the model for the backing side of electrical tape. Signals for these isotopes were used to create the scores plot in Figure 13.

Order of Variance	Isotopes
1 <sup>st</sup>	$^{121}\text{Sb}$ , $^{123}\text{Sb}$ , $^{206}\text{Pb}$ , $^{207}\text{Pb}$ , $^{208}\text{Pb}$
2 <sup>nd</sup>	$^{46}\text{Ti}$ , $^{47}\text{Ti}$ , $^{48}\text{Ti}$ , $^{49}\text{Ti}$ , $^{92}\text{Mo}$ , $^{95}\text{Mo}$ , $^{96}\text{Mo}$ , $^{98}\text{Mo}$ , $^{135}\text{Ba}$ , $^{137}\text{Ba}$
3 <sup>rd</sup>	$^{56}\text{Fe}$ , $^{66}\text{Zn}$ , $^{68}\text{Zn}$ , $^{78}\text{Sr}$ , $^{80}\text{Sr}$ , $^{78}\text{Se}$ , $^{80}\text{Se}$ , $^{209}\text{Bi}$

The orders of variance listed in Table 5 indicate that ultratrace elements such as Mo and Bi contribute to the variance in the scores plots. These elements are easily recognizable, vary between the brands, and could be transferred to tape by roller contact during the manufacturing process. Molybdenum and Bi have not been measured in electrical tapes in previous studies (such as those from Goodpaster<sup>17</sup> and Mehlretter<sup>15</sup>) possibly because they are not deliberate additives in the bulk manufacturing process. This information regarding Bi and Mo content could have otherwise been overlooked were it not for the sensitivity and elemental coverage of ICP-MS and the large data management of PCA combined with the iterative subtraction technique.

These additives were found to be three of the handful of elements which contributed the most to the variance between different brands for the backing side of electrical tape. Each manufacturer of electrical tape could have its own “recipe” of additives, making brand comparison easier.

From Figure 14, the average Q-residual values for all brands fall above the 95% confidence value when compared to models created from each brand. This indicates all brands of the backing side of electrical tape analyzed here are distinguishable from one another to 95% confidence.

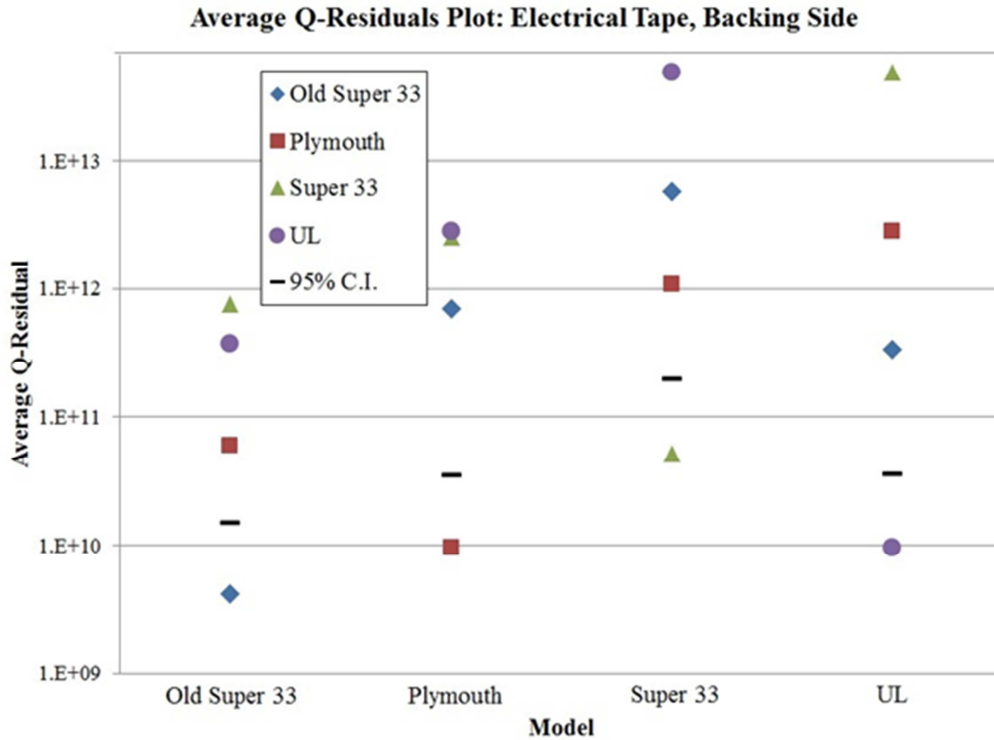
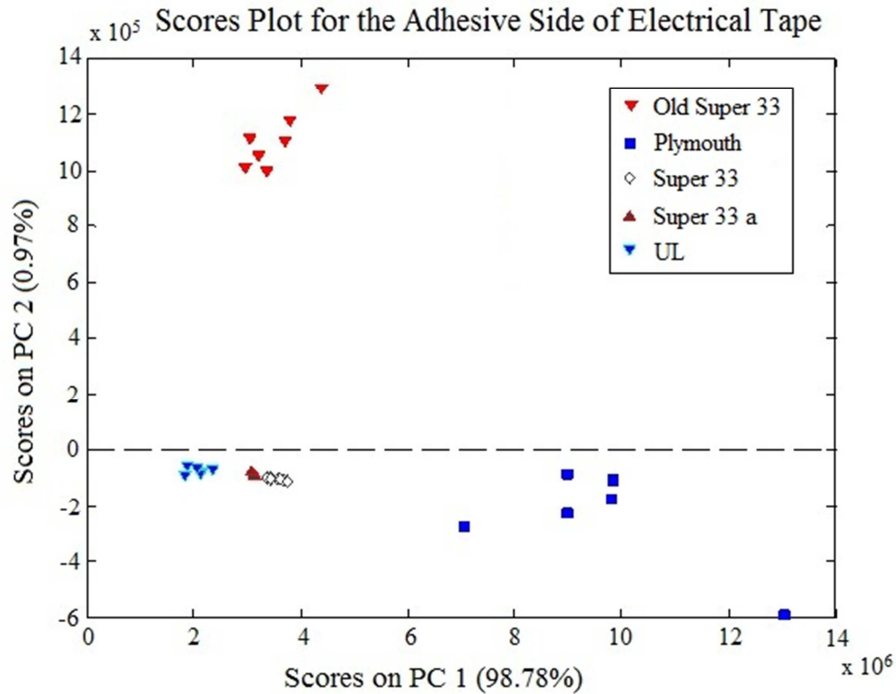


**Figure 14** Average Q-residuals plot for the backing side of electrical tape. The black line denotes the 95% confidence interval for each model.

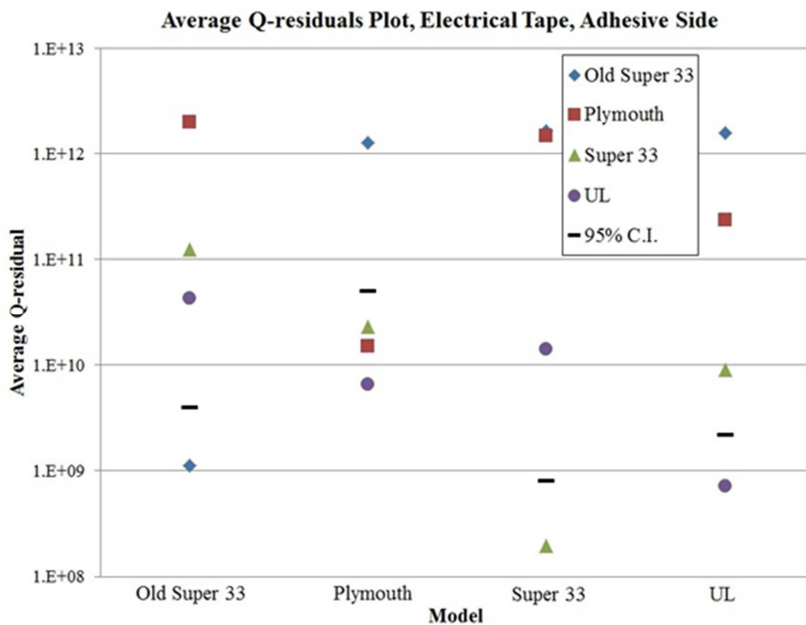
### *Electrical Tape, Adhesive Side*

Figure 15 is the scores plot for the adhesive side of electrical tape. This side of electrical tape is usually a thin layer of adhesive that is unevenly painted or sprayed onto the backing. This layer is so thin that it is difficult to ablate without sampling the backing side as well. Thus, results from the adhesive side are likely to contain elements from both the adhesive and backing sides.

Figure 16 is the average Q-residuals plot for each brand of tape. When Plymouth brand tape is used as the model, that brand cannot be distinguished from UL and Super 33 to 95% confidence, which can be explained by Figure 15.



**Figure 15** Scores plot for the adhesive side of electrical tape. The numbers in the parentheses indicate the amount of variance captured in the principal component. The model was based on elements contained in the first three orders of variance.



**Figure 16** Average Q-residuals plot for the adhesive side of electrical tape. The black line denotes the 95% confidence interval for each model.

At first glance, the scores for each brand of tape seem to be easily distinguishable from one another. However, the scores for Plymouth brand (blue squares) are spread out, pushing the 95% confidence interval value further out to overlap the points of both UL and Super 33 scores.

When Super 33 is used as the model, the Q-residuals values for the other brands (Old Super 33, UL, and even Plymouth) are distinguishable to 95% confidence. The scores for Super 33 brand tapes cluster very close in one region of the scores plot, making the 95% confidence interval very small. Scores from other brands do not fall within the 95% confidence interval for Super 33 brand tapes, even though they are in close proximity. The scores for UL brand behave similar to those of Super 33. Although the average Q-residual values indicate that UL, Super 33 and Plymouth brands are indistinguishable from one another to 95% confidence, Figure 16 does show that Super 33, Old Super 33 and UL brands are distinguishable from one another to 95% confidence. These results highlight the importance of using different sets of results as the model to thoroughly assess possible differences in samples.

The iterative subtraction of data for elements contributing the most variance to the backing side of these brands was performed and elements corresponding to the first three orders of variance may be found in Table 6. Given the nature of the adhesive side application and the difficulty in analyzing solely the adhesive side, it is difficult to make any conclusions regarding those elements which contribute the most variance to the adhesive side only.

**Table 6** Variance contribution of elements to the model for the adhesive side of electrical tape. Signals for these isotopes were used to create the scores plot in Figure 15.

Order of Variance	Isotopes
1 <sup>st</sup>	$^{46}\text{Ti}$ , $^{47}\text{Ti}$ , $^{48}\text{Ti}$ , $^{49}\text{Ti}$ , $^{56}\text{Fe}$ , $^{121}\text{Sb}$ , $^{123}\text{Sb}$ , $^{206}\text{Pb}$ , $^{207}\text{Pb}$ , $^{208}\text{Pb}$
2 <sup>nd</sup>	$^{31}\text{P}$ , $^{66}\text{Zn}$ , $^{68}\text{Zn}$ , $^{78}\text{Se}$ , $^{80}\text{Se}$ , $^{135}\text{Ba}$ , $^{137}\text{Ba}$ , $^{140}\text{Ce}$ , $^{142}\text{Ce}$
3 <sup>rd</sup>	$^{51}\text{V}$ , $^{52}\text{Cr}$ , $^{53}\text{Cr}$ , $^{63}\text{Cu}$ , $^{65}\text{Cu}$ , Zr, $^{78}\text{Sr}$ , $^{80}\text{Sr}$ , $^{118}\text{Sn}$ , $^{120}\text{Sn}$ , $^{139}\text{La}$ , $^{209}\text{Bi}$

## CONCLUSION

An iterative subtraction technique was used to identify the elements that contributed the most to the distinction between different brands of tape. This provides information that complements that from a standard multivariate statistical data analysis technique such as PCA. A successful head-to-head elemental analysis of the backing and adhesive sides of duct tape was demonstrated using iterative subtraction applied with PCA. This method was applied to both the backing and adhesive sides of duct tape. All brands of duct tape analyzed here were distinguishable from one another.

From Tables 3 and 4, the Al signal is captured in the 1<sup>st</sup> order variance in both the adhesive and backing sides of duct tapes. This indicates that the amount of Al varies greatly in duct tapes. The level of Al in could be used as a quick diagnostic to rapidly differentiate between different brands of duct tape.

The method described here was also applied to both sides of electrical tape. The technique was successful at distinguishing all brands from one another only for the *backing* side. However, analysis for the adhesive side highlighted the importance of varying the set of results that are used as the model. Additionally, it is likely that all brands could not be distinguished from one another for the adhesive side of electrical tape due to difficulties sampling only the adhesive. The very thin, uneven nature of the adhesive side on electrical tape could have been a limiting factor of accurately analyzing this side.

PCA in conjunction with iterative subtraction to determine elemental variance contribution has been shown here to be useful in distinguishing between different brands of tapes. This method has been shown to identify important, distinctive elements that are not immediately obvious from mass spectra; these distinctive elements are not necessarily the most abundant ones. The process provides extra information of potential forensic value.

The use of biplots to supplement conventional PCA may serve as an additional tool for forensic scientists when performing trace elemental analysis of tapes. The method used here could also be applied to other forms of evidence. Similar trace elemental analysis studies of other common forms of evidence collected at crime scenes such as paints, and glass could be useful to forensic scientists.

Although fs laser ablation ICP-MS has been shown to decrease fractionation and melting effects caused by sample heating,<sup>8</sup> our fs laser ablated completely through the tape too rapidly. This is why the ns laser was used for the study described above.

## **PROGRESS PART II**

### **SAMPLING AND SPATIAL HETEROGENEITY**

#### **IN TRACE ELEMENTAL ANALYSIS OF COPPER WIRE**

#### **FOR FORENSIC PAIRWISE COMPARISONS**

##### **Abstract**

The objective of this work is to assess the forensic value of copper wire strands for pair wise comparison based on trace element composition. Speaker cable, typically comprised of multiple strands of copper wire, is commonly used for binding or strangling victims and is often left at crime scenes. Fragments may also be recovered after a bomb explosion. Comparing the elemental composition of fragments of copper wire strands recovered from crime scenes to that of strands found on or near a suspect could be useful evidence in a trial. Numerous strands of varying lengths from a multi-strand speaker cable were analyzed using laser ablation-inductively coupled plasma-mass spectrometry (LA-ICP-MS). Multivariate statistical analysis was performed on the mass spectra to determine the compositional variability within a particular wire strand and between different strands. Spatial homogeneity of the trace elemental composition within a sample must be determined in order to verifiably distinguish recovered fragments from other strands. The copper wire strands in this study are spatially heterogeneous in trace element composition. The spatial variability in the trace elemental composition within a single strand of copper wire is similar to that between multiple strands. Examining spatially resolved data is important to determine the variations in elemental composition within a sample. In actual forensic

applications, the possibility of spatial heterogeneity must be considered, especially in cases where only small samples (e.g., copper wire strand fragments after an explosion) are available.

## **Introduction**

Inductively coupled plasma-mass spectrometry (ICP-MS) offers the potential for a highly sensitive, relatively non-destructive, rapid, and cost effective analysis of small samples for identification and comparison of forensic evidence.<sup>33,34</sup> Trace and ultratrace elemental analysis by ICP-MS has been used to determine if samples are similar to or distinguishable from one another. This technique has been used for various samples of steel and glass, including float, container, sheet, and automotive glass for forensic analysis.<sup>20, 33, 35, 36</sup> LA-ICP-MS was used to distinguish between gold samples and also determine the provenance of the samples.<sup>1</sup> Other samples such as gemstones, soils, and car paints have also been distinguished from similar samples based on trace elemental composition measured with LA-ICP-MS.<sup>23,37,38,39</sup> The provenance has also been determined for samples such as cannabis crops, oriental porcelain, and others using LA-ICP-MS to measure trace elemental composition.<sup>34,40,41</sup>

However, not all forensic samples can be clearly distinguished from each other based on trace elemental composition using LA-ICP-MS. Further investigation into compositional analysis of bullet lead by the Federal Bureau of Investigation (FBI) and the National Research Council (NRC) suggested specific guidelines for the analysis of bullet lead.<sup>42</sup> It was determined that anywhere from 12,000 up to 35 million bullets from a 40-grain .22 caliber long rifle may be produced from “compositionally indistinguishable volumes of lead” (CIVL). Many bullet manufacturers also add scrap lead from the bullet production to melt at random times which sporadically changes the composition of the original melt.<sup>42</sup>

One recent development in laser ablation ICP-MS is the use of femtosecond lasers, which produce more accurate, precise and reproducible isotopic measurements compared to nanosecond lasers, particularly for metals.<sup>5</sup> Finer particulates created with femtosecond ablation lead to an increase in signal intensity and stability, and narrower confidence intervals for determining unknown concentrations when ablating solid metal targets compared to a nanosecond laser.<sup>5,43,44</sup> When glass is ablated with a femtosecond laser, higher signal intensity, better internal precision, repeatability, and accuracy were observed compared to a nanosecond laser.<sup>4</sup>

The improvement in the results with femtosecond ablation is due to the reduction of fractionation that occurs during ablation. Fractionation causes a measured signal ratio for different elements that is not representative of the ablated sample composition. Imprecision caused by fractionation during the laser ablation process is common. A thorough explanation of elemental fractionation during laser ablation has been described in other work.<sup>45,46</sup> Fractionation is reduced when using a femtosecond laser, which minimizes sample heating and often produces smaller particles, at least for some sample matrices.<sup>5,43,44,45,47</sup> When helium is used though the ablation cell instead of argon, a decrease in deposition around the ablation pit, an increase in signal intensities, and an improvement in the limit of detection are observed.<sup>45,48</sup> A femtosecond laser with helium though the ablation cell coupled to the ICP-MS can provide a more accurate measurement of trace elements with high sensitivity and selectivity.

Data analysis methodology is also important in forensic analysis. One valuable chemometric method is principal component analysis (PCA), which reduces multivariate data into a simple, two-dimensional scores plot. The scores plot depicts most of the variation within a data set. PCA has been proven to be a

useful, efficient, and reproducible technique for the comparison of forensic samples by trace elemental composition with LA-ICP-MS.<sup>20,26,38,41</sup>

Speaker cable, which is typically comprised of copper wire, is commonly used for binding, strangulation at crime scenes, or to make bombs. Comparison of one or more copper wire strands found at a crime scene to ones found on a suspect could be used as evidence to link the suspect to the scene of the crime.

In this project, preliminary work determined individual strands of copper wire had different trace elemental compositions and could apparently be distinguished from one another.<sup>26</sup> These initial studies formed the basis of the present work. The spatial variability of the elemental composition of the copper wire strands was further investigated. This paper illustrates an issue in sampling size of the strands for pair-wise comparisons which is caused by the spatial heterogeneity of the trace elemental composition within a copper strand. Spatial heterogeneity results were verified by solution analysis.

## Methods

### *Samples*

Ten copper strands were unwound from 30 meters of Monster XP Compact High Performance Speaker Cable wire and were used in this study. The Monster XP speaker cable wire was coated with a linear polyethylene dielectric (LPE) insulation. The LPE insulation was peeled off the wire. Then ten copper strands were unbraided from the 65 stranded wire. In this paper, the term “wire” refers to the entire speaker cable, a bundle of copper strands intertwined together and covered with a plastic insulation. A “strand” is a single copper thread removed from the insulation and unwound from the wire. A “segment” of a strand is a section from which one or multiple “sub segments” (~ 9 cm long / piece) of strand were removed for analysis (Fig. 1). The same ten copper strands were used in all experiments and are labeled accordingly Strand 1-10.

### *Laser Ablation Analysis*

LA-ICP-MS was used to analyze the copper strands. An apparatus to pull the strands straight in the ablation cell was developed to allow for the laser to remain on the strand during the ablation. A sub segment of the copper strand, 2 cm in length, was ablated. Each sub segment of copper strand removed for analysis

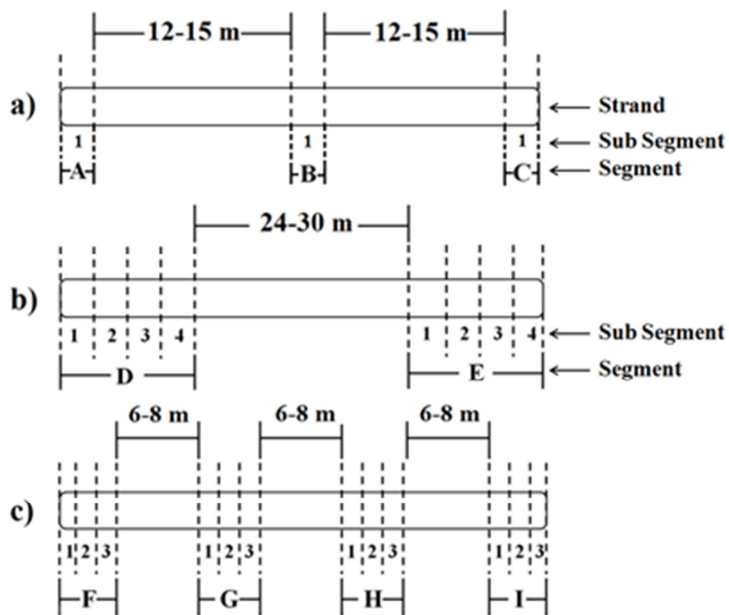


FIG. 1—Diagrams of the segments and sub segments removed from copper wire strands for analysis. Figure 1a) describes the first experiment explained in the paper for laser ablation analysis. Figure 1b) describes the second experiment in this paper for laser ablation analysis. Figure 1c) is a diagram of the sub segments removed for sample dissolution analysis.

was  $\sim 9$  cm long to allow for room to grasp the strand to mount it in the apparatus. The diameter of a copper strand was approximately  $120 \mu\text{m}$ .

Two types of laser ablation experiments are presented. The experiments are listed in order of the number of sub segments per strand which were analyzed, not in the chronological order they were performed. In Experiment A, one sub segment ( $\sim 9$  cm long) of three segments (A, B, and C) of nine copper strands was removed for analysis (Fig. 1a). In Experiment B, four adjacent sub segments ( $\sim 9$  cm long pieces) of two segments (D and E) of ten copper strands were removed for analysis (Fig. 1b). Multiple laser ablation experiments were conducted, which all yielded similar results. The two laser ablation experiments presented in this paper provide an accurate representation of the results from many such experiments done over the duration of the project.

In both experiments, the sub segments were ablated with a femtosecond (fs) (Coherent Libra Ti:Sapphire 266 nm, Santa Clara CA) laser in a single line scan pattern. Helium gas was used as the carrier gas through the ablation cell. The nominal spot size of the femtosecond laser was  $\sim 50 \mu\text{m}$ . The laser removed roughly the upper half of each wire, leaving the remaining strand with a semi-circular, D-shaped cross section. Attempts to re-ablate such a strand were not successful. Thus, the figures of merit of different laser (i.e., the fs vs a more conventional ns laser) could not be compared directly on the same strands.

The strands were suspended  $\sim 1$  cm above a piece of Teflon so the edge of the laser that did not ablate the strand was defocused before it reached the Teflon piece. Argon was introduced into the sample tube after the ablation cell and before the torch via a Y setup. The elemental mass spectra were acquired using a magnetic sector ICP-MS (Element I, Thermo Scientific Inc., Bremen Germany). Plasma conditions were optimized with a tune solution for maximum and most stable signals (Table 1). In Experiment A, 45 mass spectra were measured per sub segment of each strand. Signals for the  $m/z$  values of Ag, Bi, Cu, Mo, Pb, Sb, Sn, W, Zn and Zr were peak-area integrated and background subtracted. In Experiment B, due to the large number of sub segments, 12 mass spectra per sub segment were measured. Signals for the  $m/z$  values of Ag, Cu, Pb, Sb, Sn, Zn and Zr were peak-area integrated and background subtracted. In both experiments the background was measured with

**Table 1** Instrument and laser parameters for the analysis of copper wire strands

ICP-MS Instrument	Element 1 (Thermo Finnigan, inc.)
10 ns Laser	CETAC LSX 500 Nd:YAG
Operational wavelength	266 nm
Laser energy	9.1 mJ pulse <sup>-1</sup>
Frequency	20 Hz
Spot size	100 μm
Raster speed	80 μm sec <sup>-1</sup>
100 fs Laser	Coherent Libra Ti:Sapphire
Operational wavelength	266 nm
Laser energy	140 mW pulse <sup>-1</sup>
Frequency	1000 Hz
Spot size	~50 μm
Raster speed	80 μm sec <sup>-1</sup>
Sampler and skimmer cones	Ni, X configuration (Thermo, inc.)
Carrier gas through ablation cell	0.800 ± 0.19 L He min <sup>-1</sup>
Additional gas after laser, before torch	0.530-0.550 L Ar min <sup>-1</sup>
RF Power	1150 W
Outer gas flow	16.00/1.16 L Ar min <sup>-1</sup>
Torch position, ion optics	Optimized for maximum sensitivity and stability
Scan mode	Peak jump, 1 point per mass, 10 ms dwell time, 2.1 ms settling time
dwell/settling time	
Acquisition	
Runs/passess	15 (ns laser) or 45 (fs laser) runs/1 pass
Resolution	Low

the laser on, shutter closed, and helium flowing through the ablation cell. Bi, Mo, and W were included to the original list of elements after detected in various dissolution samples of copper wire strands.

Numerous experiments were also conducted on the copper wire strands using a nanosecond (ns) laser (LSX 500 Nd:YAG 266 nm, CETAC Technologies, Omaha NE). Results were similar with either laser; however, only the fs laser results are reported below. In particular, the spatial heterogeneity described below was of similar severity with either laser.

Measures were taken to account for various instrumental effects. All copper strands from each experiment were analyzed on the same day to eliminate day to day plasma variations. A piece of standard NIST 610 glass was ablated with the fs laser and selected m/z values were measured at the beginning and end of each experiment and compared to monitor for instrument drift over time. Signals for the selected m/z values were normalized to the  $^{63}\text{Cu}^+$  signal to correct for the variations in the amount of copper strand removed during ablation. To address possible problems caused by copper deposition on the cones, m/z values were normalized to the  $^{63}\text{Cu}^+$  signal and new background spectra were measured frequently. The new background spectrum was subtracted from the succeeding mass spectra acquired from the following copper strands.

Various laser ablation experiments were performed with the femtosecond laser to eliminate possible sources of variations in trace element signals other than heterogeneity of the strand. Different methods of cleaning the strand were performed on the strand before ablation. Strands were wiped with either a dry Kimwipe, or a Kimwipe wetted with D.I. water, or ablated with the femtosecond

laser to remove the surface of the strand before the mass spectra were acquired. The mass spectra from the cleaned strands were compared to mass spectra from strands where no cleaning was performed. There was no significant difference in the mass spectra between the cleaned strands and the strands which were not cleaned (data not shown). Experiments were also conducted to account for the variation which may be introduced when the ablated strands are removed from the apparatus in the ablation stage and new strands are added. No significant difference in the mass spectrum from a set of strands in the ablation stage to the next was observed (data not shown).

### *Sample Dissolution Analysis*

Segments of copper strands were also dissolved to eliminate possible errors due to laser ablation, such as fractionation. Sample dissolution was used as a validation method for the LA-ICP-MS results. Three sub segments of four segments, (F, G, H, and I) of five copper wire strands were broken by hand (i.e. not cut with a metal object) every 6 to 8 meters (Fig. 1c). Each sub segment of copper strand was weighed to 0.01 g and dissolved in 1 g of 70 percent nitric acid. The nitric acid was purified by sub boiling distillation. The solution was diluted to ~100 ppm copper and 0.7 percent nitric acid with Millipore water. Gallium and indium were added at 1 ppb as internal standards. The solutions were prepared in Teflon bottles which were cleaned by vapor above 70% nitric acid for at least 16 hours. The solutions were introduced with a 100  $\mu\text{L}/\text{min}$  self aspirating nebulizer (PFA 100, ESI Analytical) and analyzed with the ICP-MS. Signals for the m/z values of Ag, Cu, Ga, In, Pb, Sb, Sn, Zn and Zr were peak-area integrated and background subtracted. There was a substantial copper background signal; however it was still four orders of magnitude smaller than the  $\text{Cu}^+$  signal from dissolved copper in the samples.

*Data Analysis for Comparison of Strands.*

PCA has been reviewed in detail elsewhere.<sup>49</sup> In short, PCA reduces multivariate data into a simple, two dimensional scores plot which depicts most of the variation within the data set. The scores plot is composed of a set of axes called principal components (PCs). The PCs represent the major variance within the variables (net signals at selected m/z values) of a data set. A PCA scores plot allows for the visualization and interpretation of the samples in the data set in comparison to one another.<sup>26</sup>

Data sets comprising multiple mass spectra from one, or multiple, sub segments of a copper strand, were used to produce a PCA scores plot. This data set is referred to as the model. Data sets from the sub segments of the remaining copper strands were compared to the model. The difference, or variance, of the data set from the model was determined by the Q-value. The Q-value is a measure of the difference, or residual, between the mass spectra of one data set to their projection onto the model in the PC scores plot.<sup>26</sup> A large Q-value indicates the data set differs extensively from the PCA model. The multiple Q-values of a data set are averaged together to simplify the plot and depict an overall point that represents the average Q-value for a copper strand. A 95% confidence interval (C.I.) is created from each model. If the average Q-value of a strand is larger than the Q-value of the 95% C.I. of the model, the copper strand is distinguishable from the model. Alternatively, if the average Q-value of a copper strand is smaller than the Q-value of the 95% C.I. of the model, the copper strand and the model are indistinguishable from one another to a 95% C.I. To simplify the data, tables were created which list the strands that were indistinguishable from the PCA model based on the average Q-value of the strand and the 95% C.I. of the model.

The strands that are not listed in a particular table were distinguishable from the model.

For laser ablation results, signals were normalized to the  $^{63}\text{Cu}^+$  signal and the Cu signals were removed from the PCA analysis. For the dissolution results, signals were normalized to that for  $^{63}\text{Cu}^+$ , the ratio was then corrected using the internal standards. Cu, Ga, and In signals were removed from the PCA analysis. Commercial software, Solo Eigenvector version 6.5.1 was used for the PCA. No other scaling or preprocessing was used before data were input to the PCA software.

## **Results and Discussion**

### *Laser Ablation*

Two sub segments of a copper wire strand were ablated with the femtosecond laser and all selected elements were measured with the ICP-MS (Fig. 2). Seven elements with the largest signals that contained more than one isotope and minimum interferences were initially selected for experiments. The selected elements included Cu, Zn, Zr, Ag, Sn, Sb, and Pb. Bi, Mo, and W were included in later experiments after they were found in various copper strands. Examination of the various isotope ratios shows that all these signals are due to the actual atomic ions and are not polyatomic interferences.

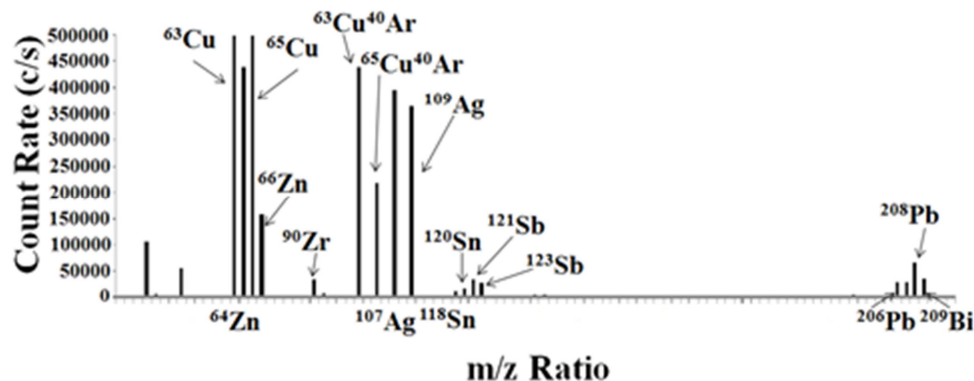


FIG. 2—Average mass spectrum for two copper wire strands ablated with the fs laser and measured on the Thermo Finnigan Element ICP-MS. Peaks with significant count rates (c/s) were labeled, m/z ratios were measured from  ${}^7\text{Li}$  to  ${}^{238}\text{U}$ . Peaks below m/z 63 were not labeled due to polyatomic interferences.

### *Experiment A: Pairwise Comparison of Segments A, B, and C between Nine Copper Wire Strands*

Three segments (A, B, and C) per copper strand were ablated with the femtosecond laser. The mass spectra from segment (A) of one strand are used as the model in an average Q-residual plot and compared to the mass spectra of segment A from the remaining strands. This comparison is repeated with segment (A) of each strand used as the PCA model. The Q-values from each mass spectrum were averaged together to represent the average Q-value for that strand. The strands which were indistinguishable from the PCA model (average Q-value was lower than the Q-value from the 95% C.I. of the model) in the average Q-residual plot are listed in Table 2. Most of the strands are distinguishable from one another in the pair-wise comparisons. There are only six total indistinguishable pair-wise comparisons when the mass spectra from one sub segment of segment A are used as the model for comparisons (Table 2). Results are similar when the mass spectra from the sub segments of segment B and C are used as the models for comparison in an average Q-residual plot (data not shown).

**Table 2 Experiment A: Comparison of Segment A.** Numbers under “PCA Model” column correspond to the strand from which the mass spectra of segment A were used to produce the PCA model. The mass spectra from segment A of the strands listed in the “Indistinguishable Strand/s” column are indistinguishable from the strand in the PCA model to a 95% C.I.

<b>PCA Model</b>	<b>Indistinguishable Strand/s</b>
1	-
2	4, 9
3	-
4	-
5	9
7	5
8	-
9	-
10	4, 9

Next, the mass spectra from the sub segments of segments A, B, and C of a strand were included in the model. The mass spectra from the three segments of the remaining strands are compared to the model. The Q-values from the three sub segments in each strand were averaged together to represent the average Q-residual for a strand. The strands which were indistinguishable from the model are listed in Table 3. When the distance over which the copper strand is analyzed increases from one sub segment to three sub segments, the total number of indistinguishable pair-wise comparisons increases to eight. Note in Table 3 Strand 8 is indistinguishable from six of the models. This is because the compositional variability within the mass spectra of the segments in Strand 8 is larger than the variability within most of the other strands in this experiment. This is explained in more detail at the end of the Results/ Discussion section.

**Table 3 Experiment A: Comparison of All Segments.** Numbers under “PCA Model” column correspond to the strand from which the mass spectra of segment A, B and C were used to produce the PCA model. The mass spectra from segment A, B, and C of the strands listed in the “Indistinguishable Strand/s” column are indistinguishable from the strand in the PCA model to a 95% C.I.

PCA Model	Indistinguishable Strand/s
1	-
2	8
3	8
4	8
5	8
7	8, 2
8	-
9	1
10	8

*Experiment A: Pairwise Comparison of Sub Segments within an Individual Strand*

Based on the previous results, many of the copper strands seem to be distinguishable from one another based on trace element composition. The mass spectra of one segment are compared to the mass spectra from the remaining segments within the same strand in an average Q-residual plot (Fig. 3).

Unfortunately, segments of the same strand are also distinguishable from one another. The differences between the segments within the same strand are of the same magnitude as the difference between strands in the previous average Q-residual plots. The results from the segments not shown in the graph are also distinguishable from one another within the same strand; they are not shown to simplify the plot.

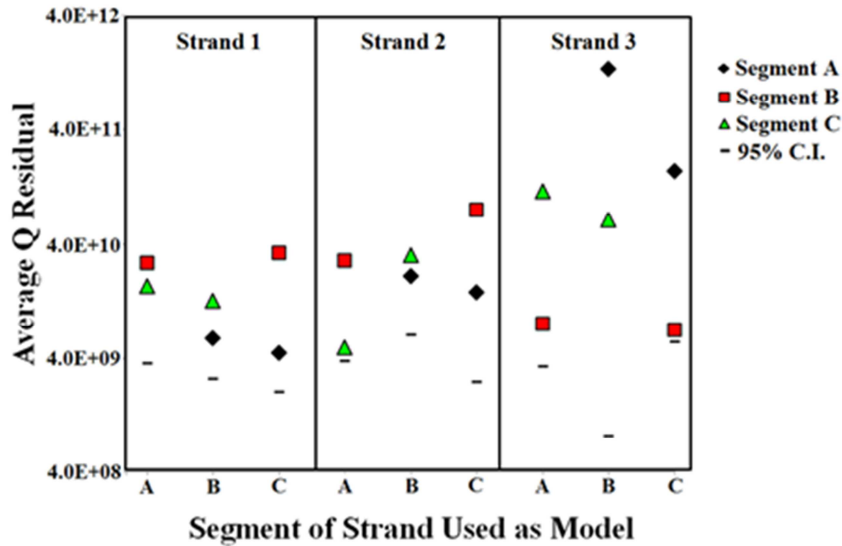


FIG. 3—Average Q residual plot from one segment (A, B, or C) of nine copper wire strands. The segments in each box originate from the strand numbered at the top of each box. The segments from the remaining six strands not shown in plot are also distinguishable from one another within the same strand. Wire strands were ablated with a 100 femtosecond laser and measured on the Element ICP-MS.

Signals of each element measured during the laser ablation were plotted versus distance over which the strand was ablated. Spikes in the signals of the  $m/z$  values measured are mainly due to actual spatial variations in the trace elemental composition within the 2 cm long copper strand (Fig. 4). The laser ablated the 2 cm piece of copper strand over 4.5 minutes while the ICP-MS scanned through the selected  $m/z$  values. The large spikes in element signal occur over 10 seconds or more of the analysis and are not merely due to large particles entering the plasma. A small time lapse occurs between isotope measurements as the magnet scans over the mass-to-charge ratios. However, even considering the small time lapse, many of the elements do not occur together throughout the strand. It appears that certain elements are present mainly in discrete grains or inclusions and are not distributed homogeneously.

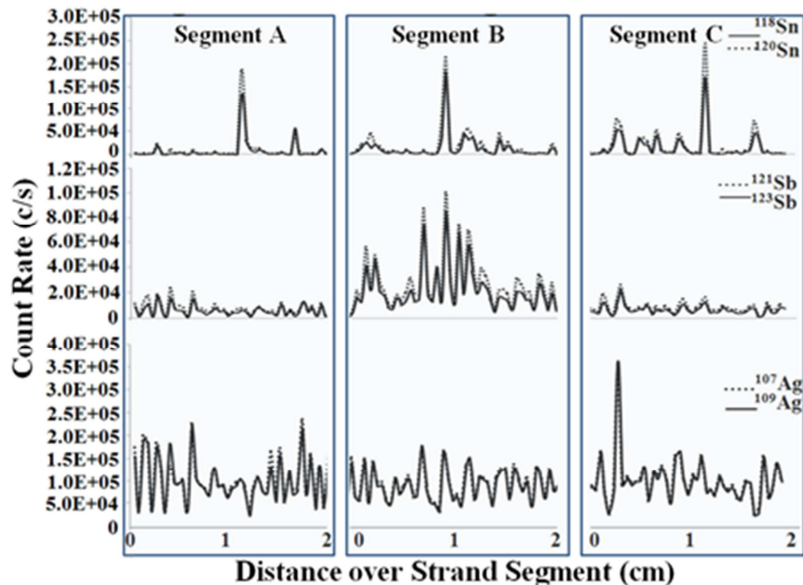


FIG. 4—Plot of count rate (c/s) vs. distance ablated over a strand segment (cm). Segment A, B, and C were removed between 12-15 meters throughout a strand. 45 scans of the selected isotopes were measured on the Element ICP-MS over 275 seconds as the laser ablated over the 2 cm of the strand. Results were similar with the remaining m/z ratios measured. Wire strands were ablated with the fs laser. Signals are normalized to  $^{63}\text{Cu}^+$  signal.

These results indicate that the spatial variability of the trace elemental composition throughout a copper wire strand is similar to the variability between different strands. Time resolved isotope signals over a length of a sample are useful in order to indicate the heterogeneity of the sample. Many other data sequencing methods do not collect time and spatially resolved data. Due to the trace elemental heterogeneity within a single strand, analysis of one small fragment of a strand will not be an adequate sample size to distinguish between strands or wires.

#### *Experiment B: Effects of Heterogeneity on an Increased Sample Size*

A larger number of sub segments were analyzed in order to determine the effects of heterogeneity on an increased sampling size. Four sub segments of segment D and E were ablated with the Libra femtosecond laser (Fig. 1b). Eight

sub segments per strand were sampled in this experiment compared to the three sub segments analyzed in the previous experiment. Mass spectra from four sub segments of segment D of a strand were compared to those from the four sub segments of segment D from the remaining strands. With a larger area of copper strand for comparison, the total number of indistinguishable pair-wise comparisons increases to 43 (Table 4). The results are similar when the four sub segments of segment E of a strand are compared to the sub segments of segment E of the remaining strands in an average Q-residual plot (plot not shown).

**Table 4 Experiment B: Comparison of Four Sub Segments from Segment D.** Numbers under “PCA Model” column correspond to the strand from which the mass spectra of four sub segments from segment D were used to produce the PCA model. The mass spectra from four sub segments from segment D of the strands listed in the “Indistinguishable Strand/s” column are indistinguishable from the strand in the PCA model to a 95% C.I.

PCA Model	Indistinguishable Strand/s
1	9, 5, 8, 2
2	-
3	1, 2, 5, 8, 9, 10
4	1, 2, 3, 5, 8, 9, 10
5	2, 8, 9, 10
6	1, 2, 3, 4, 5, 7, 8, 9, 10
7	1, 2, 5, 8, 9, 10
8	2, 9, 10
9	5, 10
10	2, 9

The increase in the number of indistinguishable pair-wise comparisons compared to Experiment A may be due to the number of sub segments per segment used for analysis. An increase in the number of sub segments of copper wire

strand leads to an increase in the spatial variability of the trace elemental composition. The increase in spatial variability is due to the heterogeneity of the trace elemental composition within the strand. Using four sub segments as the PCA model in the average Q-residual plot increases the variability within the model. With larger variability within the model, segment D of the remaining strands becomes less distinguishable from the Q-residual model.

Mass spectra of the eight sub segments from segment D and E are included in the Q residual model and compared to the sub segments from segment D and E of the remaining strands (Table 5). There are 44 indistinguishable pair-wise comparisons when eight sub segments of a strand are compared to eight sub segments of the remaining strands in an average Q-residual plot. Again, an increase in the spatial variability of the trace elemental composition over longer distance of copper strand analyzed causes more strands to become indistinguishable from one another based on the average Q-residual plot.

**Table 5 Experiment B: Comparison of All Sub Segments.** Numbers under “PCA Model” column correspond to the strand from which the mass spectra of all sub segments were used to produce the PCA model. The mass spectra from all sub segments of the strands listed in the “Indistinguishable Strand/s” column are indistinguishable from the strand in the PCA model to a 95% C.I.

<b>PCA Model</b>	<b>Indistinguishable Strand/s</b>
1	2, 3, 4, 5, 8, 9, 10
2	3, 5
3	5, 8, 9, 10
4	3, 5, 8, 9, 10
5	8
6	3, 4, 5, 8, 9, 10
7	3, 4, 5, 6, 8, 9, 10
8	5, 9, 10
9	3, 4, 5, 8, 10
10	3, 5, 8, 9

*Experiment B: Pairwise Comparison of Segments D, and E within an Individual Strand*

The four sub segments from segment D are compared to the four sub segments of segment E within the same strand in an average Q-residual plot (Fig. 5). The segments of Strand 1 are distinguishable from one another. In the remaining strands, the segments are distinguishable from one another (the average Q value falls above the 95% C.I.) when one segment is used as the model. However, when the opposite segment of the same strand is used as the model, the segments appear indistinguishable from one another (the average Q value falls below the 95% C.I.). This result is caused by the spatial variability of the trace

elemental composition within the segment used as the model. When the spatial variability in the sub segments used as the PCA model is larger than that of the sub segment the model is compared to, the two segments are indistinguishable from one another in an average Q-residual plot. Note the larger Q value of the 95% C.I. in the model when the two segments are indistinguishable. This is another indication that the model has a larger variation with more spatial variability within the sub segments. Likewise, the two segments appear distinguishable from one another when the spatial variability in the trace elemental composition of the sub segments in the model is smaller than that of the sub segments the model was compared to. These results also indicate that the spatial variability of the trace elemental composition within a single copper wire strand is similar to the variability between strands.

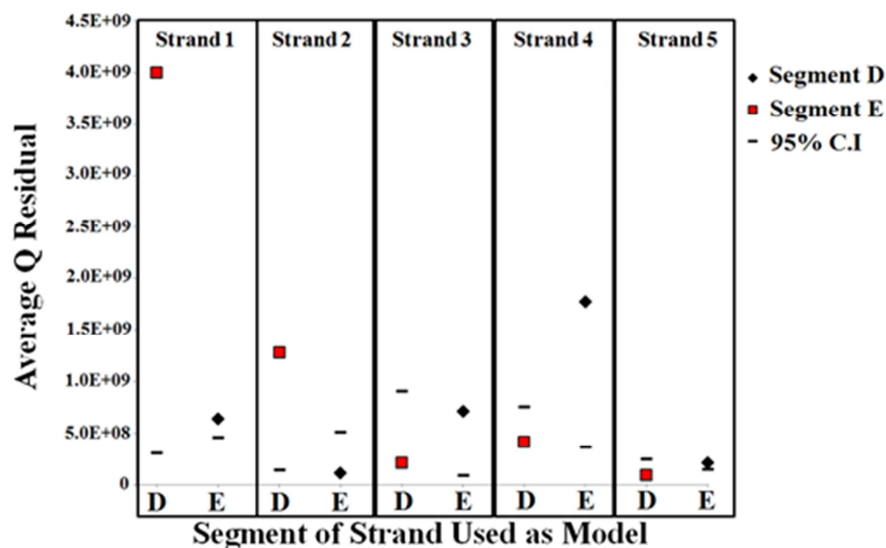


FIG. 5—Average Q residual plot from one segment (D or E) of ten copper wire strands. The segments in each box originate from the strand numbered at the top of each box. The remaining five strands not shown in plot follow the same trend as the plots above. Wire strands were ablated with the fs laser and measured on the Element ICP-MS.

All of the trace elements measured contribute to the spatial variability within a model to different degrees depending on the sub segment. For example, the sub

segment used as one of the models may have large Pb and Sn signal spikes increasing the variability within that model. The sub segments used for another model could have large Sb and Zn signal spikes, which would increase the variability within that particular model. These sub segments may originate from the same copper wire strand, which explains why segments from the same strand are distinguishable as well as indistinguishable from one another depending on which segment is used for the model. For example, when segment D, in Strand 2 (Fig. 5) is used as the model; segment E from the same stand appears distinguishable from the model. Segment E from Strand 2 has large Sn and Sb signal spikes. This increases the variability within the model for segment E compared to segment D resulting in segment E being distinguishable from segment D. Conversely, when segment E from Strand 2 is used as the PCA model, segment D is indistinguishable from the model in the Q-residual plot. This again is due to the large variability within the model of segment E. Large variability within the data set used as the model causes more data sets to become indistinguishable from the model. Therefore, heterogeneity of the sample and sampling size must be considered in order to confirm an indistinguishable pair or distinguish two samples from one another based on trace elemental composition.

An important observation from this study is that when more sub segments are included in the PCA model of a Q-residual plot, more strands become indistinguishable from the model in a pair-wise comparison. The increase in the number of indistinguishable pair-wise comparisons is due to an increase in the variation within the PCA model. This is the result of large differences in the data used for the PCA model. Variation in the data, in this particular case, is a result of fluctuations in the signals of the various  $m/z$  values measured during laser ablation of the copper strands. Examples of large variations in PCA models include the PCA model of Strand 8 in Table 3, as well as the Q-residual plot for segment

comparison of Strands 2-6 in Fig 5. Multiple effects may cause fluctuations in the signals of the various  $m/z$  values. Spatial heterogeneity throughout the copper strand will cause fluctuations in the signal at various  $m/z$  values. The more area (or sub segments) included into the PCA model, the more signal fluctuation is introduced, unless very large areas of the sample are analyzed. This creates a large PCA model which leads to more indistinguishable strands in a pair-wise comparison to the PCA model. Other sources of signal fluctuation were considered and measures were taken to account for those fluctuations explained in the Experimental section.

### *Dissolution Experiments*

Variability within and between strands could be merely due to the laser ablation process. Therefore, dissolved samples were analyzed to eliminate laser ablation variability from the data. Dissolved samples of three sub segments of four segments (F, G, H, and I) of five strands of copper wires were measured on the Thermo Finnigan Element ICP-MS to validate the laser ablation results (Fig. 1c). All twelve of the sub segments from the dissolution samples of a strand were compared to the twelve sub segments of the remaining dissolution samples of the other four strands in an average Q-residuals plot (Fig. 6). In the comparison of five strands, there are nine indistinguishable pair-wise comparisons. These results verify the laser ablation results, twelve sub segments of a single strand increase the variability in the model. Larger variability within the model causes indistinguishable pair-wise comparisons based on the trace element composition.

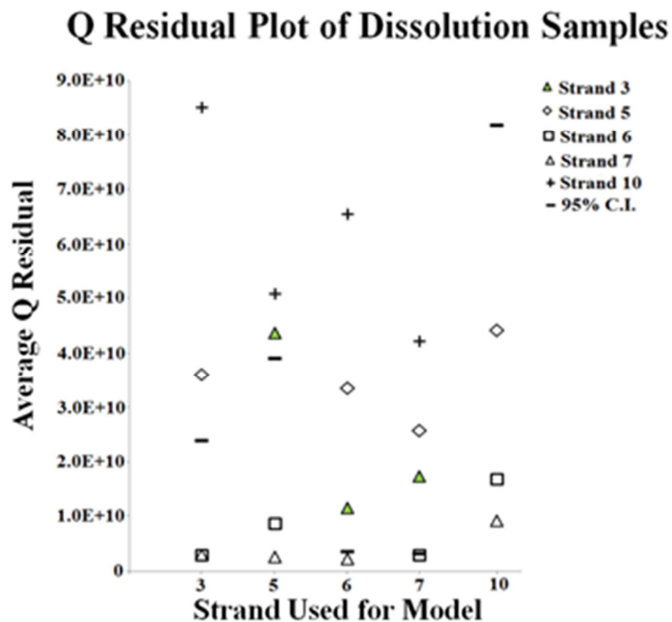


FIG. 6—Average Q residual plot for three sub segments of the four segments (F, G, H, and I) of five copper wire strand dissolution samples. This plot verifies the laser ablation results that many of the strands are indistinguishable from one another based on trace elemental composition.

In a PCA scores plot ten replicate measurements of each of the twelve sub segments were acquired with ICP-MS. The ten replicates of each sub segment cluster together in the PCA score space. Replicates or samples which cluster in similar score space in a PCA scores plot are considered similar, or indistinguishable. However, most of the sub segments within the same strand cluster in separate score space (Fig. 7). The separate clustering of the sub segments within a single strand indicates the sub segments are dissimilar, or distinguishable from one another. This verifies that the trace elemental composition of a copper strand varies significantly within short distances (~10 cm) between sub segments within the same segment of a single strand.

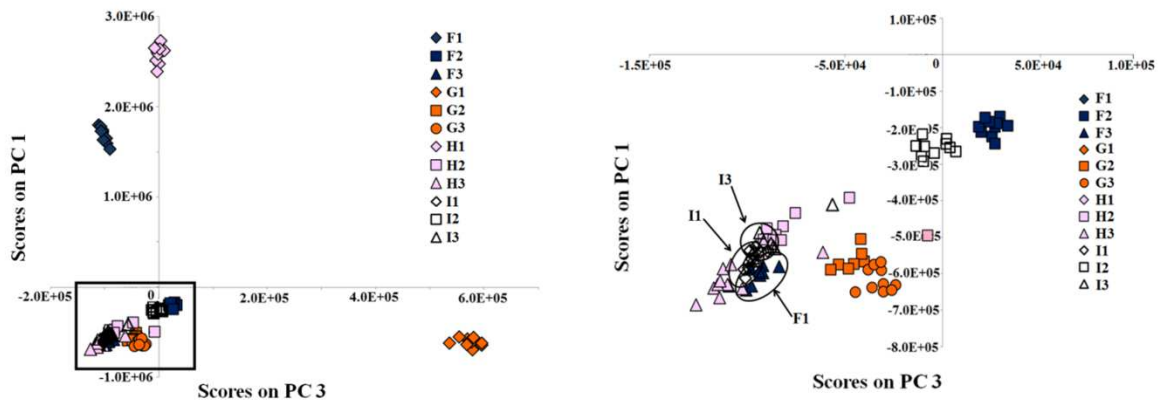


FIG. 7—Scores plots for the dissolved samples of three sub segments of four segments, (F, G, H, and I) from strand number ten. The boxed area from the left plot is enlarged in the second PCA plot at right. Sub segments F3, H2, H3, I1, and I3 cluster together and are indistinguishable. I3, I1, and F1 are circled to better indicate the grouping, the circles are not indicative of a confidence interval. The remaining sub segments cluster separate from one another in score space indicating sub segments of the same strand are distinguishable.

To further indicate the variation in the trace elemental composition over a short distance, a plot of the average signal of the ten replicate measurements from three dissolution sub segment samples of Strand 10 were plotted in a graph (Fig. 8). The signals were background subtracted, normalized to the  $^{63}\text{Cu}^+$  signal, and multiplied by  $1 \times 10^{11}$  to return the signal to the original magnitude. Some of the signals are up to two times larger in one sub segment compared to another. These three sub segments were removed from less than 40 cm of Strand 10. This is

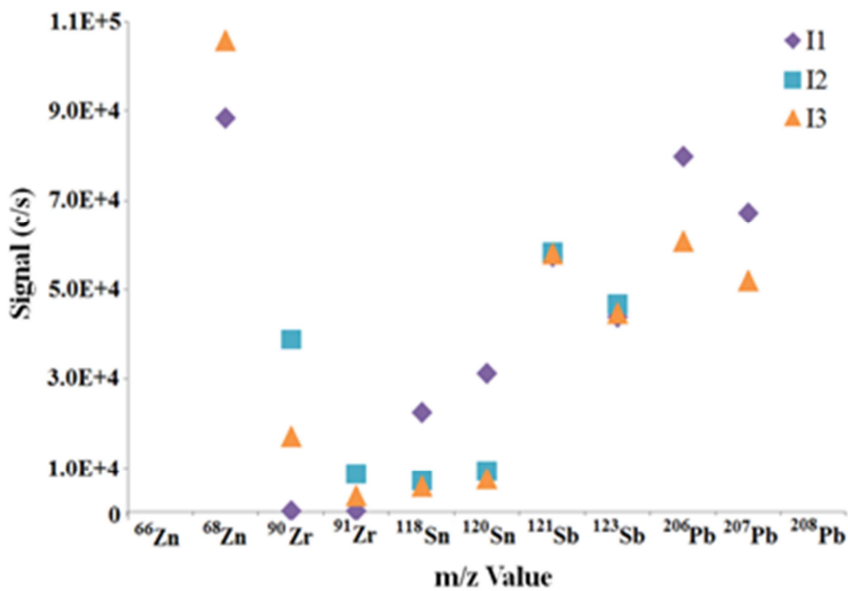
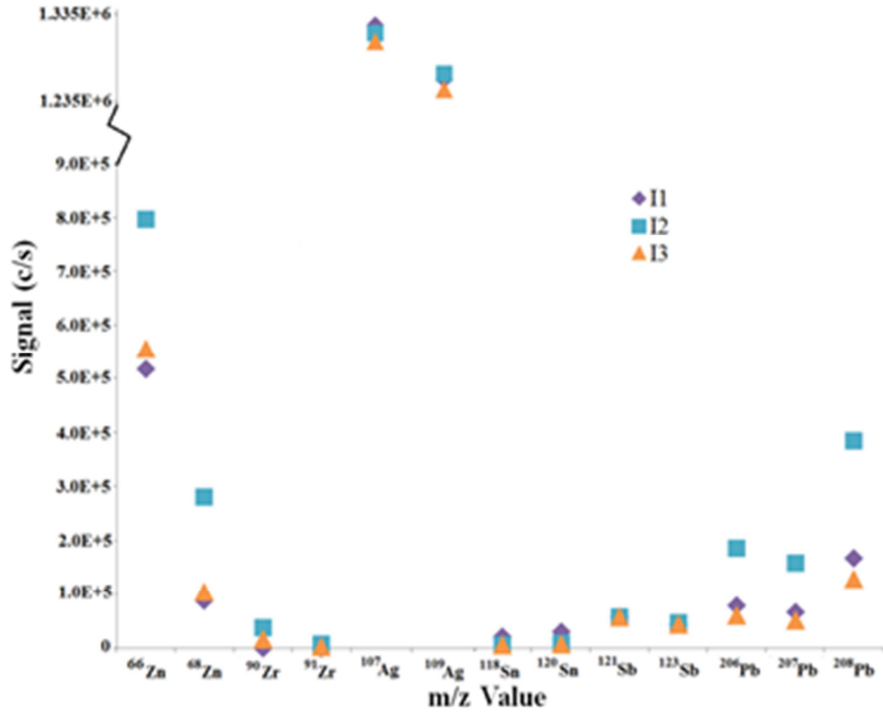


FIG. 8—Signals at measured  $m/z$  values of the sub segments I1, I2, and I3 of Strand 10. The second graph is the same graph as above with the maximum y-axis zoomed in to  $1.1 \times 10^5$ . Silver  $m/z$  values were removed from the x-axis on the second graph because the signals were larger than the y-axis maximum.

another representation of large variations in trace element composition over a short distance in a strand. Notice, in the PCA scores plot (Fig. 7), sub segments I1, I2, and I3, are clustered the closest to one another in the score space compared to the other sub segments within segments F, G, and H. The closer the sub segments cluster in score space, the more similar the sub segments. Sub segments I1, I2, and I3 are the most similar sub segments within a single segment on the PCA scores plot. Similar results were obtained for signal plots of the other sub segments (data not shown).

Sample contamination must be considered in the dissolution samples and may account for some separation of the samples in the score space. However, the likeliness of variable contamination in every dissolution sample of Strand 10 is considered small. Therefore, most of the separation in score space is likely due to spatial variability in the elemental composition throughout a strand. Thus, the observation of large spatial heterogeneity using laser ablation is confirmed by the dissolution experiments. PCA plots of the remaining four strands produced similar separation of samples in score space (data not shown).

## **Conclusion**

This study shows that the spatial variability, or homogeneity, of the trace elemental composition within a sample should be determined in order to verifiably distinguish recovered fragments from other strands. Examining spatially resolved data is important to verify the variations in elemental composition within a sample. This is an example of a case where averaging data points together for comparison between samples does not adequately represent the entire sample. When a small number of sub segments from a copper strand are analyzed the results indicate

most of the strands are distinguishable from one another in pair-wise comparisons. However, when sub segments throughout 30 m of the copper strand are analyzed many of the strands are no longer distinguishable due to the spatial variability of the trace elemental composition throughout a single copper strand. Individual segments within a single strand are also distinguishable from one another in an average Q-residual plot, indicating spatial variability throughout a strand. When the spatial variability in the trace elemental composition used as the PCA model in an average Q-residual plot increases, more strands become indistinguishable by pair-wise comparisons from the PCA model. The variations in the elemental composition along the length of a strand are similar to the variations between different strands. The heterogeneity of the sample and sampling size must be considered in order to confirm an indistinguishable pair, or distinguish two samples from one another based on trace elemental composition.

In actual forensic applications, the possibility of spatial heterogeneity should be evaluated, especially in cases where only small samples (e.g., copper wire strand fragments after an explosion) are available. It may be helpful to investigate the manufacturing process more closely to determine the cause of the heterogeneity throughout a copper strand, similar to the research performed on manufacturing processes of container glass and compositional analysis of bullet lead (CABL).

42,50

## **DISSEMINATION OF RESEARCH FINDINGS**

The project represents much of the Ph.D thesis of Megan Mekoli, which was approved in November 2012. It comprises the initial parts of the thesis of Jonna Berry, which should be finished in approximately 2015. At least two journal publications are being prepared from this material. The work was presented at two conferences, as indicated below.

Oral Talk – Mekoli, M.L.; Berry, J.E.; Bock, M.K.; Jacobs, J.L.; Bajic, S.J.; Houk, R.S. Improvements in LA-ICP-MS for Trace Forensic Analysis of Common Household Products Using a Short (100 Femtosecond) Pulse Ultraviolet Laser. Presented at the Trace Evidence Symposium, Kansas City, MO, August 11, 2011. Megan's talk

Poster - Berry, J.; Bajic, S. J.; Houk. R. S. Determination of the Spatial Variability of the Elemental Composition of Copper Wire using Inductively Coupled Plasma-Mass Spectrometry, Young Forensics Science Forum, Atlanta GA, 2012.

## References

1. Watling, R. J.; Herbert, H. K.; Delev, D.; Abell, I. D. Gold Fingerprinting by Laser Ablation Inductively Coupled Plasma Mass Spectrometry. *Spectrochimica Acta Part B: Atomic Spectroscopy* **1994**, *49B*, 205-219.
2. Trejos, T.; Montero, S.; Almirall, J. R. Analysis and Comparison of Glass Fragments by Laser Ablation Inductively Coupled Plasma Mass Spectrometry (LA-ICP-MS) and ICP-MS. *Anal. Bioanal. Chem.* **2003**, *376*, 1255-1264.
3. Hattendorf, B.; Latkoczy, C.; Günther, D. Laser Ablation-ICPMS. *Anal. Chem.* **2003**, *75*, 341A-347A.
4. Poitrasson, F.; Mao, X. L.; Mao, S. S.; Freydier, R.; Russo, R. E. Comparison of Ultraviolet Femtosecond and Nanosecond Laser Ablation ICP-MS Analysis on Glass, Monazite, and Zircon. *Anal. Chem.* **2003**, *75*, 6184-6190.
5. Liu, C.; Mao, X. L.; Mao, S. S.; Zeng, X.; Greif, R.; Russo, R. E. Nanosecond and Femtosecond LA of Brass: Particulate and ICPMS Measurements. *Anal. Chem.* **2004**, *76*, 379-383.
6. Wang, Z.; Hattendorf, B.; Günther, D. Vaporization and Ionization of Laser Ablation Generated Aerosols in an Inductively Coupled Plasma Mass Spectrometer - Implications from Ion Distribution Maps. *J. Anal. At. Spectrom.* **2006**, *21*, 1143.
7. Pisonero, J.; Günther, D. Femtosecond Laser Ablation Inductively Coupled Plasma Mass Spectrometry: Fundamentals and Capabilities for Depth Profiling Analysis. *Mass Spectrom. Reviews* **2008**, *27*, 609-623.
8. Koch, J.; Günther, D. Femtosecond Laser Ablation Inductively Coupled Plasma Mass Spectrometry: Achievements and Remaining Problems. *Anal. Bioanal. Chem.* **2007**, *387*, 149-153.
9. Aeschliman, D. B.; Bajic, S. J.; Bladwin, D. P.; Houk, R. S. High-Speed Digital Photographic Study of an Inductively Coupled Plasma During Laser

- Ablation: Comparison of Dried Solution Aerosols from a Microconcentric Nebulizer and Solid Particles from Laser Ablation. *J. Anal. At. Spectrom.* **2003**, *18*, 1008.
10. Saetveit, N. J.; Bajic, S. J.; Baldwin, D. P.; Houk, R. S. Influence of Particle Size on Fractionation with Nanosecond and Femtosecond Laser Ablation in Brass by Online Differential Mobility Analysis and Inductively Coupled Plasma Mass Spectrometry. *J. Anal. At. Spectrom.* **2008**, *23*, 54.
  11. Pisonero, J.; Kock, J.; Wälle, M.; Hartung, W.; Spencer, N. D.; Günther, D. Capabilities of Femtosecond Laser Ablation Inductively Coupled Plasma Mass Spectrometry for Depth Profiling of Thin Metal Coatings. *Anal. Chem.* **2007**, *79*, 2325-2333.
  12. Bradley, M. J.; Keagy, R. L.; Lowe, P. C.; Rickenbach, M. P.; Wright, D. M.; LeBeau, M. A. A Validation Study for Duct Tape End Matches. *J. Forensic Sci.* **2006**, *51*, 504-508.
  13. Keto, R. O. Forensic Characterization of Black Polyvinyl Chloride Electrical Tape. *Crime Lab Digest* **1984**, *11*, 71-74.
  14. Kee, T. G. The Characterization of PVC Adhesive Tape. *Proceedings of the International Symposium on the Analysis and Identification of Polymers*, Quantico, VA; Washington D.C., 1984.
  15. Mehlretter, A. H.; Bradley, M. J.; Wright, D. M. Analysis and Discrimination of Electrical Tapes Part II: Backings. *J. Forensic Sci.* **2011**, *56*, 1493-1504.
  16. Hida, M.; Satoh, H.; Mitsui, T. Comparative Study of A Cluster Analysis and A Principal-Component Analysis Using a Polarized Imaging Technique for Discriminating Adhesive Cloth Tapes. *Anal. Sci.* **2002**, *18*, 717-722.
  17. Goodpaster, J. V.; Sturdevant, A. B.; Andrews, K. L.; Brun-Konti, L. Identification and Comparison of Electrical Tapes Using Instrumental and Statistical Techniques I: Microscopic Surface Texture and Elemental Composition. *J. Forensic Sci.* **2007**, *52*, 610-629.

18. Goodpaster, J. V.; Sturdevant, A. B.; Andrews, K. L.; Briley, E. M.; Brun-Konti, L. Identification and Comparison of Electrical Tapes Using Instrumental and Statistical Techniques II: Organic Composition of the Tape Backing and Adhesive. *J. Forensic Sci.* **2009**, *54*, 328-338.
19. Gray, A. L. Solid Sample Introduction by Laser Ablation for Inductively Coupled Plasma Source Mass Spectrometry. *Analyst* **1985**, *110*, 551-556.
20. Bajic, S. J.; Aeschliman, D. B.; Saetveit, N. J.; Baldwin, D. P.; Houk, R. S. Analysis of Glass Fragments by Laser Ablation-Inductively Coupled Plasma-Mass Spectrometry and Principal Component Analysis. *J. Forensic Sci.* **2005**, *50*, 1123-1127.
21. Weis, P.; Deucking, M.; Watzke, P.; Menges, S.; Becker, S. Establishing a Match Criterion in Forensic Comparison Analysis of Float Glass Using Laser Ablation-Inductively Coupled Plasma-Mass Spectrometry. *J. Anal. Atom. Spec.* **2011**, *26*, 1273-1284.
22. May, C. D.; Watling, R. J. A Comparison of the Use of Refractive Index (RI) and Laser Ablation-Inductively Coupled Plasma-Mass Spectrometry (LA-ICP-MS) for the Provenance Establishment of Glass Bottles. *Forensic Sci. Med. and Path.* **2009**, *5*, 66-76.
23. Guillong, M.; Gunther, D. Quasi "Non-destructive" Laser Ablation-Inductively Coupled Plasma-Mass Spectrometry Fingerprinting of Sapphires. *Spectrochimica Acta Part B: Atomic Spectroscopy* **2001**, *56B*, 1219-1231.
24. Scheid, N.; Becker, S.; Duecking, M.; Hampel, G.; Volker Kratz, J.; Watzke, P.; Weis, P.; Zauner, S. Forensic Investigation of Brick Stones Using Instrumental Neutron Activation Analysis (INAA), Laser Ablation-Inductively Coupled Plasma-Mass Spectrometry (LA-ICP-MS), and X-ray Fluorescence Analysis (XRF). *Appl. Rad. and Iso.* **2009**, *67*, 2128-2132.
25. Bebe, K. R.; Pell, R. J.; Seasholtz, M. B. *Chemometrics: A Practical Guide*. John Wiley & Sons: New York, 1998; pp 81-112.
26. Aeshliman, D. B.; Bajic, S. J.; Baldwin, D. P.; Houk, R. S. *Multivariate Pattern*

- Matching of Trace Elements in Solids by Laser Ablation-Inductively Coupled Plasma-Mass Spectrometry: Source Attribution and Preliminary Diagnosis of Fractionation. *Anal. Chem.* **2004**, *76*, 3119-3125.
27. SWGMAT. Guidline for Forensic Examination of Pressure Sensitive Tapes. <http://www.swgmat.org/Pressure%20Sensitive%20Tape%20guideline.pdf> (accessed February 2012).
28. Braeunling, E. *Handbook of Pressure Sensitive Tapes*, 3rd ed.; Van Norstrand Reinhold: New York, 1999; pp 643-660.
29. Houk, R. S.; Fassel, V. A.; Flesch, G. D.; Svec, H. J.; Gray, A. L.; Taylor, C. E. Inductively Coupled Argon Plasma as an Ion Source for Mass Spectrometric Determination of Trace Elements. *Anal. Chem.* **1980**, *52*, 2283-2289.
30. Jolliffe, I. T. *Principal Component Analysis*, 2nd ed.; Springer: New York, 2002.
31. Shlens, J. A Tutorial on Principal Component Analysis Derivation, Discussion and Singular Value Decomposition, 2003. [http://www.cs.princeton.edu/picasso/mats/PCA-Tutorial-Intuition\\_jp.pdf](http://www.cs.princeton.edu/picasso/mats/PCA-Tutorial-Intuition_jp.pdf) (accessed November 2, 2012).
32. Jolliffe. Chapter 5: Graphical Representation of Data Using Principal Components. In *Principal Component Analysis*, 2nd ed.; Springer: New York, 2002; pp 78-110.
33. Watling, R. J.; Lynch, B.; Herring, D. Use of Laser Ablation Inductively Coupled Plasma Mass Spectrometry for Fingerprinting Scene of Crime Evidence. *J. Anal. At. Spectrom.* **1997**, *12*, 195-203.
34. Watling, R. J. Sourcing the Provenance of Cannabis Crops Using Inter-Element Association Patterns 'Fingerprinting' and Laser Ablation Inductively Coupled Plasma Mass Spectrometry. *J. Anal. At. Spectrom.* **1998**, *13*, 917-926.
35. Suzuki, Y.; Kikkawa, H. S.; Kasamatsu, M.; Higashikawa, Y.; Suzuki, S. Forensic Discrimination of Sheet Glass Exposed to High Temperature by the Determination of Trace Impurities Using ICP-MS. *Anal. Sci.* **2008**, *24*, 745-

749.

36. Naes, B.; Umpierrez, S.; Ryland, S.; Barnett, C.; Almirall, J. A Comparison of Laser Ablation Inductively Coupled Plasma Mass Spectrometry, Micro X-ray Fluorescence Spectroscopy, and Laser Induced Breakdown Spectroscopy for the Discrimination of Automotive Glass. *Spectrochimica Acta Part B: Atom. Spec.* **2008**, *63*, 1145-1150.
37. Watling, J. R.; Herbert, H. K.; Barrow, I. S.; Thomas, A. G. Analysis of Diamonds and Indicator Minerals for Diamond Exploration by Laser Ablation-Inductively Coupled Plasma Mass Spectrometry. *Analyst* **1995**, *120*, 1357-1364.
38. Arroyo, L.; Trejos, T.; Hosick, T.; Machermer, S.; Almirall, J.; Gardinali, P. Analysis of Soils and Sediments by Laser Ablation Inductively Coupled Plasma Mass Spectrometry (LA-ICP-MS): An Innovative Tool for Environmental Forensics. *Environ Forensics* **2010**, *11*, 315-327.
39. Deconinck, I.; Latkoczy, C.; Günther, D.; Govaert, F.; Vanhaecke, F. Capabilities of Laser Ablation-Inductively Coupled Plasma Mass Spectrometry for (Trace) Element Analysis of Car Paints for Forensic Purposes. *J. Anal. At. Spectrom* **2006**, *21*, 279-287.
40. Bartle, E.; Watling, J. R. Provenance Determination of Oriental Porcelain Using Laser Ablation-Inductively Coupled Plasma-Mass Spectrometry. *J. of Forensic Sci.* **2007**, *52*, 341-348.
41. Green, R.; Watling, R. J. Trace Element Fingerprinting of Australian Ocher Using Laser Ablation Inductively Coupled Plasma-Mass Spectrometry (LA-ICP-MS) for the Provenance Establishment and Authentication of Indigenous Art. *J. of Forensic Sci.* **2007**, *52*, 851-859.
42. National Research Council (U.S.) CoSAoBLECC. *Forensic Analysis: Weighing Bullet Lead Evidence*; National Academies Press: Washington, D.C, 2004.
43. Margetic, V.; Pakulev, A.; Stockhaus, A.; Bolshov, M.; Niemax, K.; Hergenröder, R. A Comparison of Nanosecond and Femtosecond Laser-

- Induced Plasma Spectroscopy of Brass Samples. *Spectrochim. Acta Part B: Atom. Spec.* **2000**, *55*, 1771-1785.
44. Možná, V.; Pisonero, J.; Holá, M.; Kanický, V.; Günther, D. Quantitative Analysis of Fe-based Samples Using Ultraviolet Nanosecond and Femtosecond Laser Ablation-ICP-MS. *J. Anal. At. Spectrom* **2006**, *21*, 1194-1201.
45. Kuhn, H. R.; Günther, D. Elemental Fractionation Studies in Laser Ablation Inductively Coupled Plasma Mass Spectrometry on Laser-Induced Brass Aerosols. *Anal. Chem.* **2003**, *75*, 747-753.
46. Trejos, T.; Almirall, J. R. Effect of Fractionation on the Forensic Elemental Analysis of Glass using Laser Ablation Inductively Coupled Plasma Mass Spectrometry. *Anal. Chem.* **2004**, *76*, 1236-1242.
47. Chichkov, B. N.; Momma, S.; Nolte, S.; von Alvensleben, F.; Tünnermann, A. Femtosecond, Picosecond, and Nanosecond Laser Ablation of Solids. *Appl. Phys. A* **1996**, *63*, 109-115.
48. Günther, D.; Heinrich, C. A. Enhanced Sensitivity in Laser Ablation-ICP Mass Spectrometry Using Helium-Argon Mixtures as Aerosol Carrier. *J. Anal. At. Spectrom.* **1999**, *14*, 1363-1368.
49. Beebe, K. R.; Pell, R.; Seasholtz, M. B. *Chemometrics; A Practical Guide*; Wiley: New York, 1998.
50. Harrington, K. J.; Land, D. P.; Pollock, E. M.; Springer, F. A.; Howitt, D. G. Forensic Development of LA-ICP-MS: Elemental Profiling and Evaluation of Homogeneity in Soda-Lime Container Glass, 2012. Projects at nfstc: Science Serving Justice. <http://projects.nfstc.org> (accessed December 4, 2012).